5-2019

Polymeric PVDF Fibers for Piezoelectric Applications in Energy Harvesting

Misael E. Martinez
The University of Texas Rio Grande Valley

POLYMERIC PVDF FIBERS FOR PIEZOELECTRIC APPLICATIONS IN ENERGY HARVESTING

A Thesis

by

MISAEL E. MARTINEZ

Submitted to the Graduate College of
The University of Texas Rio Grande Valley
In partial fulfillment of the requirements for the degree of

MASTER OF SCIENCE IN ENGINEERING

May 2019

Major Subject: Mechanical Engineering

POLYMERIC PVDF FIBERS FOR PIEZOELECTRIC APPLICATIONS IN ENERGY HARVESTING

A Thesis
by
MISAEL E. MARTINEZ

COMMITTEE MEMBERS

Dr. Karen Lozano
Chair of Committee

Dr. Horacio Vasquez
Committee Member

Dr. Javier Ortega
Committee Member

May 2019

ABSTRACT

Martinez, Misael E., Polymeric PVDF Fibers for Piezoelectric Applications in Energy Harvesting. Master of Science in Engineering (MSE), May, 2019, 89 pp., 8 tables, 33 figures, references, 79 titles.

This work focuses on developing and characterizing the piezoelectric response of Cerium doped Polyvinylidene Fluoride (PVDF) fine fibers and the effects of dopants and alignment on the formation of the β-phase and consequently on the piezoelectric performance. Six sets of fiber mats were prepared varying the concentration (2.5-7.5wt%) of Cerium (III) Nitrate-Hexahydrate and Ammonium-Cerium (IV) Sulfate-Dihydrate. Fiber mats were developed using the Forcespinning® technique and the angular velocity and dopant concentration were adjusted to obtain a synergy between fiber yield and fiber diameter. Fourier Transform Infrared Spectroscopy showed a significant enhancement in the PVDF β-phase and inhibition of the non-polar α-phase. The doping effect of the cerium complexes shows a small effect on the piezoelectric response, with the PVDF Cerium-Sulfate fibers producing 7 to 8V; whereas the pure PVDF fibers' response ranged between 5 to 7V. Fibers doped with 5wt% Cerium-Sulfate showed the best fiber morphology and had the highest yield of production. Addition of graphene demonstrated increased in sensitivity for the fibers, while the addition of PPy helped in increasing the charge/discharge rate for the fibers' voltage response. The effect of fiber alignment proved beneficial by increasing the β-phase formation of the fibers, reducing fiber diameter, and thus producing higher voltage response, 9.20-11 V for 5wt% Cerium-Sulfate.

DEDICATION

"Commit your works to the Lord and your plans will be established. Proverbs 16:3" This work is in dedication to God first and foremost. It was only through Him that I made it until this point; He has given me the skills to continue studying and has placed the most amazing people in my path to help me fulfill this purpose. This work is also dedicated to my family—my father, mother and my sister—for they have always supported me in all I have done, and for always believing I could do anything I set my mind to.

ACKNOWLEDGEMENTS

I gratefully acknowledge the support received by NSF PREM award under grant No. DMR-1523577: UTRGV-UMN Partnership for Fostering Innovation by Bridging Excellence in Research and Student Success.

I want to thank my advisor Dr. Karen Lozano for her continuous support throughout my academic career; she has been a great mentor and supporter of my work. This work is possible thanks to her guidance and counsel; thanks to her I learned many useful skills that I am sure will help me in my professional career.

I would also like to acknowledge the members of my thesis committee, Dr. Horacio Vasquez and Dr. Javier Ortega. Their advice and constructive comments, as well as their input and guidance helped me in different aspects for development of my project. I also want to acknowledge the help of the nano-lab's administrator, Victoria Padilla; her help and contribution will always be greatly appreciated.

I also want to acknowledge all the master students that were my partners on this journey; they taught me the basic concepts on how to do research, all the way to how to operate the most complex machines and data interpretation. Thank you very much Carlos Hernandez, Jose Zuniga, Dulce Capitanachi, Ydana Virgen, Raul Barbosa, Rodolfo Becerra, Alex Castillo, Dr. Mandana Akia, Omar Torres, Homero Gonzalez, and Astrid Rodrigues for all your help and support.

TABLE OF CONTENTS

LIST OF TABLES

Page

LIST OF FIGURES

Page

CHAPTER I

INTRODUCTION

Current technology demands smaller, cheaper, lightweight, and more efficient sources of power. As power consumption increases, research on alternative energy-harvesting methods has intensified. With energy harvesting from sunlight, wind, and water, our homes and cars could eventually be powered indefinitely; however, to power small electronic devices, such as micropumps, sensors, pacemakers, and personal portable electronics, the power supplied is somewhat limited. Motion-based energy harvesting devices capable of producing energy from mechanical motion; for example, mechanical vibrations or periodic motions are an attractive alternative to develop self-powered systems.

Polyvinylidene fluoride has been extensively used for a wide array of applications, but its main contribution is in piezoelectric applications. PVDF has been a great candidate for energy harvesting devices due to its flexibility, durability, and high voltage output when strained. Since the moment of its discovery in 1962, studies have been developed regarding new methods to process it, to enhance its properties, and for its use in different applications.

Enhancement of the piezoelectric response of PVDF depends mainly on its processing; actions such as making PVDF into fibers, doping of conductive materials, and controlling fiber orientation can positively impact the piezoelectric effect of the PVDF. Although PVDF films are more common for certain applications, studies have shown that when PVDF is made into fibers it

increases the poling of the polymer which corresponds to higher piezoelectric output.

Fiber production output can be increased orders of magnitude when using the Forcespinning® technology; this innovative technology uses centrifugal forces as the main source for fiber production. The PVDF fibers are poled mechanically instead of electrically. Addition of PVDF-Ce complexes are added to the PVDF to see the effects of doping on the degree of self-poling.

The scope of this study is to enhance the piezoelectric response of PVDF Forcespun fibers by doping of Cerium-complexes and fiber alignment—in order to create light, flexible, and cost-efficient nanogenerators that can be used as an alternative method for energy harvesting/producing applications.

CHAPTER II

REVIEW OF LITERATURE

2.1-Background on energy

Since before the advent of electronics and alternative fuels, fossil fuels were the primary source of energy in the 19th century. As the population continues to increase, the supply of power to cities and people is much lower than the demand for it; consequently, the over consumption of fossil fuels since the past decades has raised concern on whether the future generations will have enough resources for them as this consumption rate continues. Likewise, the extraction, production, and consumption of fossil fuels have raised awareness of the alarming environmental consequences, such as contamination, greenhouse gases, and global warming. Thus, research on an energy source that is eco-friendly, renewable, and cost affordable is a trending topic amongst the leading scientists in the energy industry.

Current technology demands smaller, cheaper, lightweight, and more efficient sources of power. The last few decades in the field of energy harvesting have seen some challenges regarding powering of portable smart electronic devices, due to the increasing amounts of power needed to keep the device functioning properly. Increasing power and performance of portable electronic devices corresponds to increasing need of energy supply. For example, cellphone batteries in the early 2000s would last for days due to the basic functions that the cellphone provided, such as calls and in some, texts. In contrast, the increased capabilities of cellphones

such as processing more memory, handling calls, social media, and complex algorithms for applications required more power, and thus the batteries deplete much faster. As power consumption increases, research on alternative energy-harvesting methods has intensified. In simple words, energy harvesting refers to the act of using energy seen as waste; for example, heat, kinetic energy from movement, and even light, and then converting it to viable electrical energy to supply power to an electronic device efficiently. With energy harvesting from sunlight, wind, and water, our homes and cars could eventually be powered indefinitely; however, to power small electronic devices, such as micropumps, sensors, pacemakers, and personal portable electronics, the power supplied is somewhat limited [22, 32, 68].

Motion-based energy harvesting devices capable of producing energy from mechanical motion; for example, mechanical vibrations or periodic motions are an attractive alternative to develop self-powered systems [50, 75, 76]. In comparison to other energy sources such as solar, wind, thermal, etc., mechanical vibration-based energy harvesters are said to have more potential, longer lifespan, and higher power density. There are different methods for transforming mechanical vibrations into electrical energy, such as electromagnetic induction, electrostatic generation, and piezoelectric effect. Out of these methods, piezoelectricity has demonstrated to be the most promising regarding energy harvesting, due to their ability to convert applied strain energy into usable electric energy, and their ease to be integrated into a system.

Table 1. Summary of different energy sources		
Energy source	**Pros**	**Cons**
Solar energy	Non-polluting	High investment
	Most abundant source	Dependent on clear skies and sunny weather
	Systems last 15-30 years	Requires large physical space for PV cell panels
Wind energy	No emissions	Output proportional to wind speed
	Little disruption to ecosystems	High initial investment and maintenance
	Affordable and high output	Extensive land use
Hydropower	No emissions	Dams expensive to build
	Generates large amounts of power	Change of environment in the damn area
	Output can be regulated to meet demand	May be affected by drought
Natural gas	Widely available	High transport costs
	Cleanest-burning fossil fuel	Gas resources unavailable in some areas
	Combined with other fuels to decrease pollution in energy generation	Pipelines impact ecosystems

Petroleum	Basis of many products (plastics, fuel)	High CO_2 emissions
	Economical to produce	Supply may be exhausted
	Easy to transport	Environmental impact from drilling and transporting
Biofuels	Abundant supply	Source must be near usage
	Fewer emissions	Increases emissions of nitrogen oxides
	Engines can easily convert to run on biomass	Uses some fossil fuels in conversion
Coal	Abundant supply	Emits major greenhouse gases and acid rain
	Currently inexpensive to extract	Mining can be dangerous for miners
	Reliable	High environmental impact from mining and burning
Uranium	No greenhouse or CO2 emissions	Higher costs due to safety
	Efficient at energy transformation	Problem for long term storage or radioactive waste
	Reserves are abundant	Potential nuclear issues
Geothermal	Minimal environmental impact	Few geothermal fields in the world
	Efficient	Expensive to start
	Low cost after investment	Wells could be depleted

Mechanical harvesting	Abundant supply	Some energy loss to heating or discharging
	Easy to produce	Cannot be used directly/needs storage
	No environmental impact	Output varies with application and input

2.2-What is piezoelectricity?

Piezoelectricity comes from the Greek word *piezo* or *piezin*, which means to stress or to press, and *elektron*, or electricity. Thus, piezoelectricity refers to an electric voltage produced when a certain material is stressed; the corresponding strain, whether through elongation, compression, bending, or shearing produces a proportional voltage respond that we identify as electricity. [31]

Most crystalline materials such as metals, ceramics, and some polymers fall into one of the seven different crystal structure families, and one of the 14 different Bravais lattices. Some of these crystal orientations are symmetric, for example the cubic and orthorhombic families, while others are asymmetric such as triclinic and monoclinic structures. Under normal conditions, charges are distributed evenly amongst the crystal lattice making the material chemically and electronically stable, with exceptions of some regions being more polar than others. When a mechanical stress is applied to a piezoelectric material, electrical charges appear between its two opposite sides. The appearance of charges produces an electric dipole, or an imbalance in the charges of the material. For a material with a symmetrical crystal lattice or with nonpolar molecule orientations, the dipole will be smaller and thus no significant amount of voltage will result. However, on materials with asymmetric structures, the imbalance in charges creates a

bigger dipole; the stronger the dipole, the stronger the attraction between the charges or surrounding ions. Since the charges are asymmetric, the electrons in the molecules will migrate towards the more electronegative part of the solid, thus creating an asymmetric imbalance in charges, which in consequence produces a voltage response.

To quantify the dipole density or polarization of a certain material a summation of the individual dipole moments per volume of the crystallographic unit cell must be calculated [18]. The dipole density of the material is the vector field made from all the single dipoles as vectors. Dipoles close to each other tend to be aligned in regions called Weiss Domains; such domains are usually randomly oriented but can be aligned through a process called poling. During this process, a strong electric field is applied across the material, at elevated temperatures. The more aligned the dipoles are, the greater the piezoelectric effect [20]. There are many different materials that exhibit piezoelectric effects. For example, naturally occurring crystals such as Quartz, Berlinite, Sucrose, Rochelle salt, Topaz, and Lead Titanate, among others [22]. Tendons, silk, wood, enamel, dentin, and DNA are also biomaterials exhibiting piezoelectricity, these act as biological force sensors [26,27].

One interesting aspect about the piezoelectric effect is that it is reversible. A deformation causes an electrical response, and the presence of an electrical field induces a proportional mechanical response on the material. When a voltage difference is applied across the crystals of a piezoelectric material, the structure of the unit cell undergoes deformation. The added voltage places the atoms under an “electric pressure” altering the balance of the bonding forces and the electric dipoles, and in order to regain neutrality, the atoms in the unit cell must rearrange (either tense or contract) to the closest possible neutral structure. An example of this phenomena is the quartz crystal used in watches; when voltage from a battery is applied to a quartz crystal, it will

oscillate at certain frequency, thousands of times per second, in response to the applied voltage [15,17].

2.2.1-History of Piezoelectricity

The first mention of piezoelectricity remounts back to its discovery in the late 1800s by Pierre and Jacques Curie. Between 1880 and 1882, the Curie brothers were working on measuring the surface charges on certain crystals such as tourmaline, quartz, topaz, cane sugar and Rochelle salt, when this discovery was made. This effect was dubbed “piezoelectricity” to distinguish it from contact electricity (electricity generated by friction), and pyroelectricity (electricity generated by heat). The Curie brothers did not predict the reversibility of this effect, but it was later found mathematically by Lippman in 1881 using thermodynamic principles. After two years of its discovery, the European scientific community established the core of piezoelectric applications; the identification of piezoelectric crystals based on their asymmetric crystal structure, the reversible conversion between electrical and mechanical energy, and the usefulness of thermodynamics in quantifying complex relationships between mechanical, electrical, and thermal variables. By 1910, more than 20 natural crystal classes where the piezoelectric effect was observed, and 18 possible macroscopic piezoelectric coefficients were determined.

During the following years, electromagnetism continued to be the most prolific topic in the scientific community—transitioning from theory to practical applications. Consequently, studies on piezoelectricity were obscured for a moment until the middle of the Great War. During World War I, in 1917, the first real application of a piezoelectric device was developed. P. Langevin created an ultrasonic submarine detector made from 7 quartz crystals glued to two steel plates, this transducer showed to have a resonant frequency of around 50 kHz. This sonar,

as we know it today, was the first step towards a wide array of applications for piezoelectric devices such as microphones, accelerometers, ultrasonic transducers, bender element actuators, phonograph pick-ups, signal filters, and many others.

With the coming of World War II, the need to be technologically more advance than the enemy led to increasing research on a plethora of different areas in technology, medicine, weaponry, aviation, communications, and energy sources. During this time in Japan and the Soviet Union, researchers found that certain ceramic materials exhibited a dielectric constant up to 100 times higher than common piezoelectric crystals. Advances in material science during these years include development of barium titanate family of piezoceramics, and then the lead zirconate titanate family, as well as the development and understanding of perovskite structures and their electro-mechanical properties. This period marked an important moment in the history of materials science, since it was during this time that scientists developed a rational for doping the previously mentioned ceramic families with metallic impurities and other materials to alter and achieve a desired dielectric constant, stiffness, piezoelectric coefficients, increase in strength and flexibility, etc. It was the beginning of tailoring a material for a specific application.

2.3-Piezoelectric Materials

2.3.1-Piezo-ceramics

The most common piezoelectric materials are piezo-ceramics; these are polycrystalline materials with usually a perovskite structure, composed of numerous grains each one being chemically identical to each other. The orientation of grains varies from one to another, thus properties may vary slightly across the material. Among piezo-ceramics, lead-zirconate-titanate (PZT) is considered the most widely used for energy harvesting and storage applications. Other

piezo-ceramics include barium titanate ($BaTiO_3$), and potassium niobate ($KNbO_3$). Although PZT is widely used for piezoelectric applications, this material is extremely brittle, thus it causes limitations in the strain it can safely absorb before damage occurs.

2.3.2-Piezoelectric polymers.

With the increasing demand of lightweight, higher durability, and flexibility; polymers have taken the lead. In comparison to some piezo-ceramics, some piezo-polymers perform better when it comes to mechanical stability and longevity. These materials belong to a carbon-based material with long polymer chains and are characterized by their superb flexibility when compared to single crystals and ceramics. They can withstand high strain and are suitable for applications where there is a large amount of twisting and bending. Unlike ceramics, for which the crystal structure of the material creates the piezoelectric effect, in polymers the intertwined long-chain molecules attract and repel each other when an electric field is applied. Some well-known examples of piezoelectric polymers include: Polyvinylidene fluoride (PVDF), polyvinylidene fluoride-trifluoro ethylene (PVDF-TrFE), cellulose, polyamides (PA), polylactic acids (PLA), etc.; however out of all these materials, the properties and applications of PVDF have been studied extensively. This material is useful for many applications ranging from energy-related applications like transducers—whether ultrasonic, audio, or medical—to display devices, shock sensors, actuators, and pressure sensors.

2.3.3-Piezoelectric Composites.

As mentioned before, scientists nowadays can tailor the properties of materials for specific application. To modulate and enhance the piezoelectric properties of certain piezoelectric materials, composites have been developed and the best characteristics of each

component is exploited; for example, the strength of the filler with the flexibility of the matrix. Reinforced polymer composites have been studied by effectively combining the great piezoelectric properties of PZT with the mechanical flexibility of polymers. In the case of polymer-ceramic composites, the matrix and the reinforcement alter the piezoelectric properties. For example, composites with fillers in the form of particles show poor piezoelectric properties; on the other hand, composites with fillers in the form of fibers or laminates show superior piezoelectric properties as discussed by F. Narita *et al* (2018) [55].

Similarly, the doping of other materials will have a role in the production, performance, and properties of piezoelectric devices, and their effectiveness as energy harvesters.

Table 2. Summary of piezoelectric materials investigated [53]

Material	Formula	Classification
Quartz	SiO_2	Single Crystal
Lithium Niobate	$LiNbO_3$	Single Crystal
Rochelle Salt	$KNaC_4H_4O_6{\cdot}4H_2O$	Single Crystal
Berlinite	$AlPO_4$	Single Crystal
Sucrose	$C_{12}H_{22}O_{11}$	Single Crystal
Topaz	$Al_2SiO_4(F, OH)_2$	Single Crystal
Lead-Zirconate-Titanate	PZT	Ceramic
Barium Titanate	$BaTiO_3$	Ceramic
Potassium Niobate	$KNbO_3$	Ceramic
Polyvinylidene fluoride	PVDF	Polymer
Polyvinylidene fluoride-trifluoro ethylene	PVDF-TrFE	Polymer

Polylactic Acid	PLA	Polymer
Polyamides	PA	Polymer
Cellulose	$(C_6H_{10}O_5)_n$	Polymer
Tendons	$C_{65}H_{102}N_{18}O_{21}$	Polymer
Silks		Polymer
DNA		Polymer
Polyvinylidene fluoride-Zinc Oxide	PVDF-ZnO	Composite
Cellulose -Barium Titanate	$(C_6H_{10}O_5)_n$-$BaTiO_3$	Composite
Polyamides-Lead-Zirconate-Titanate	PA-PZT	Composite

2.4-Properties

2.4.1-Properties of PVDF

Polyvinylidene fluoride, also known as PVDF or PVF_2, is one of the most well-known polymers used in piezo-, ferro- and pyroelectric applications. Discovered in 1969, this polymer demonstrated having a strong ferroelectric character. PVDF has been widely studied for the development of highly-sensitive microsensors due to its excellent piezoelectric properties, affordability, lightweight, chemical stability, and flexibility [28, 30-33].

The monomer for PVDF is composed of two carbon atoms and two fluorine atoms, ($-CH_2-CF_2-$), and since fluorine is more electronegative than the carbon and hydrogen atoms, it will attract most of the electrons to that side of the molecule. PVDF is a polymorphic material, meaning it exists in different conformation phases, each one having a unique set of properties. The most known phases are α, β, γ, δ, and ε phases; the piezoelectric effect of this polymer

strongly depends on its crystalline phase [63]. Although many other polymers have two similar pendant groups on the same polymer atom as PVDF, none has been found to have piezoelectric properties comparable to those of PVDF (according to Andre *et al* (1975)) [3].

PVDF can crystallize in at least three different conformations: TG^+TG^- in α and δ phases, all trans (TTT) planar zigzag in β-phase, and $T_3G^+T_3G^-$ in γ and ε phases [24, 47, 54]. Out of all the phases in which PVDF can be found, the α-phase is the most stable and predominant, according to Vazquez *et al* (2012) [73], and the only nonpolar phase. This phase is obtained by melt solidification all temperatures and is the only phase present in the raw state (powder) of the polymer. The nonpolar nature of the α-phase is due to the packing of the molecules. The lattices are oriented in such a way that the dipole components neutralize each other, thus in this phase PVDF does not exhibit piezoelectric properties.

The other phases, respectively the γ and δ-phases, are polar and can be obtained by applying a high electric field or heating above 160 °C. The phase that shows the highest polarity, and thus the highest piezoelectric behavior is the β-phase as studied by Lovinger (1983) [47]. The β-phase shows a stronger ferro-, piezo-, and pyroelectric response due to its largest spontaneous polarization, and because all its molecular chains are aligned with their dipoles pointing in the same direction. Researchers have focused on the formation of the β-phase of PVDF due to its significant commercial applications on electronic devices. However, the β-phase cannot be obtained from the melt by simple heating, but rather by mechanical drawing at temperatures below 90 °C; below this temperature, the molecules are stiff, and the forces applied can stretch the molecules to produce an all trans configuration (TTT).

It was reported by Salimi *et al* (2003, 2004) [62, 63] that the β-phase of PVDF is significantly enhanced by making the polymer into a fiber. Conventional methods used for fiber

making that are used throughout the literature are electrospinning and centrifugal or Forcespinning®.

PVDF can be used to produce many different products, whether films or fibers, each having its own set of properties as well as advantages and disadvantages over each other. Some characteristics include flexibility, high mechanical resistance, dimensional stability, homogenous piezo activity within a plane, high electric constant, and chemical stability. PVDF has a melting point of 170 °C, a glass transition temperature of -35 °C and a specific gravity of 1.78.

Regarding piezoelectric characteristics of PVDF, the effect varies depending on how and where in the PVDF film the stress is applied. Since these materials are anisotropic, piezoelectric coefficients are determined for each direction of the element. The values obtained are index X_{ij}, where 'i' corresponds to the direction of the electrical flow, and 'j' the direction of mechanical pressure. The piezoelectric coefficient 'd' is determined by the electrical charges delivered to a 1 m^2 of material when exposed to a 1Pa of pressure along the j-axis. The value is in coulomb per newton (C/N). During testing, mechanical stretching is a positive value, while compression corresponds to a negative value. [72]

2.5-Processing

2.5.1-Films

As mentioned before, PVDF films are the most common form that scientists and engineers use for piezoelectric applications; however, the method of production, and even the materials present in each film are different depending upon the application.

Yang *et al* (2015) [78] developed PVDF-TrFE thin films capacitors to enhance the piezoelectric properties by shear stress induction. A 5wt.% PVDF-TrFE solution was prepared

by dissolving polymer pellets in dimethylformamide (DMF), the solution was then spin-coated to a $Au/SiO_2/Si$ substrate. The samples were annealed for 1 hour at 140 °C producing films with thicknesses ranging between 70-100 nm. It was found that as the spin-coating speed increases, the value of the surface potential also increased, with a speed of 5000 RPM yielding a potential of -840.05 mV; the higher surface potential is attributed to a higher shear stress induced by the high spin rate, thus producing highly ordered dipole orientation in the films.

Table 3. Summary of properties of PVDF [53]

Property	Value	Units
Repeating unit	$-CH_2-CF_2-$	
Glass transition temperature	-35	°C
Melting temperature	160 - 170	°C
Curie temperature	80	°C
Amorphous density	1.74	g/cm^3
Crystalline density	2	g/cm^3
Molecular weight of repeating unit	64.03	g/mol
Specific gravity	1.78	
Thermal conductivity	0.19	W/m-K
Tensile strength	60	MPa
Modulus of elasticity	2200	MPa
Surface resistivity	$>10^{13}$	Ohm

piezo-strain constant	d_{31}= 23, d_{33}= -33	pC/N
Piezo-stress constant x10^{-3}	g_{31}=216, g_{33}=-330	V-m/N
Relative permittivity	ε_r= 12	
Electromechanical coupling factor at 1Hz	k_{31} = 12	%
Dielectric constant	10 - 15	

2.5.2-Fibers

In contrast to films, nanofibers are preferred for certain applications due to their increased surface area to volume ratio, and high length to diameter ratio according to Doshi *et al* (1995) [20]. Other worth mentioned characteristics that nanofibers possess are interconnected pores, high solvent uptake, and adequate mechanical strength, which makes them useful for applications such as wounds dressing materials, filters, proton exchange membranes fuel cells and much more, as studied by Vazquez *et al*. (2012) [73].

2.5.2-Electrospinning vs Forcespinning®

Extensive research has been presented on the process of Electrospinning (ES) and the effects it has on the creation of nanofibers. The way electrospinning works is by uniaxial stretching of a viscous polymer solution or melt in an electric field due to electrostatic repulsions between surface charges along the jet. The simplest apparatus for electrospinning consists of a syringe with a metal tip connected to a high voltage supply. Once the voltage is applied, the pendant droplet at the tip of the syringe becomes electrified and changes into a conical shape known as Taylor cone due to the electrostatic repulsion between the surface charges and the Coulombic force exerted by the electrical field. (Li, D *et al*, 2004) [44]. With enough high

voltage, the electrostatic repulsion between the surface charges overcomes the surface tension of the solution, and an electrified jet of polymer is ejected out the syringe; as the polymer extends, the solvent evaporates and leaves behind a solid fiber as studied by Andrew *et al* (2007) [4]. Although Electrospinning has been a fundamental process in the development and study of polymer nanofibers, the total production yield is low, with 0.1 grams/hour on average, thus if mass production of fibers is needed, a new method of production should be investigated.

Forcespinning® (FS), although it is a recent method of nanofiber production in contrast to Electrospinning, has proven successful as a viable method to mass produce polymeric nanofibers. Padron *et al* (2012) [57] report that FS utilizes centrifugal forces which allows for a significant increase in the yield and ease of production of nanofibers. While ES has a production yield of 0.1g/hour, FS takes the lead with a production method of 1g/min, over 600 times higher yield of nanofibers. For this method no electric fields are needed, thus if the material has a low dielectric constant is not a problem. The first step in FS is injecting the polymer solution into a specially designed spinneret. The parameters that need to be accounted for when solutions will be forcespun are the spinneret angular velocity (in RPM), the needle's orifice radius, polymer viscosity, relaxation time of material, surface tension, evaporation rate, temperature, and the distance from the collector to the spinneret orifice. Something that needs to be considered as well regarding polymer solutions is the polymer-solvent compatibility; this will determine the optimum concentrations that will produce the highest yields in nanofiber production, also influencing the morphology of the fiber and size. Once the polymer solution is inside the spinneret, the jet will be formed due to the centrifugal forces present; for fibers to be produced, the rotating forces must be greater than the surface tension of the solution. Forces too high will cause melt fracture or beads to form; having a high viscosity in the polymer solution will prevent

formation of a jet. Different studies have been performed regarding the optimum conditions for polymer nanofiber production. The parameters of importance in FS are humidity, angular speed, polymer solution concentration, spinning temperature and time. As the polymer jet is formed, the solvent evaporates and forms a fiber that is deposited on the collector. After all the polymer solution has left the spinneret, the fibers are removed from the collector.

Table 4. Comparison between Electrospinning and Forcespinning® [4, 57]

Parameters	Electrospinning	Forcespinning
Main force	Electric	Centrifugal
Production yield	0.1 g/hour	1 g/min
Morphology of fibers	smooth	smooth/rough
Fiber diameter	nm	nm to um
Voltage needed	20-40 kV	
Angular speed needed		1000-10,000 RPM

2.6-Characterization

Once nanofibers or films have been produced by either method these are characterized to determine the desired properties. Different characterization methods have been used to determine the thermal stability of the fibers, with parameters such as thermal degradation, melting temperature, transition temperature, crystallization temperature, and degree of crystallinity present. Other methods involve using X-Ray diffraction to determine the atomic structure and configuration of the nanofibers. Infrared Spectroscopy is also useful for analytical chemistry of the samples; it allows for easier identification of functional groups and its configuration and

concentration within the sample. This test is key in determining whether solvents have evaporated or left traces behind, and whether—depending on the configuration of the functional groups—the material created will have the desired properties. Other characterization method relies on statistical analysis for fiber diameter; using SEM pictures of the tested sample, with a measurement program, the diameter of the fibers can be measured, and average diameter calculated. Likewise, using the SEM, the morphology of the fibers can be seen, whether it is a rough or a smooth texture; whether the fiber is covered in other element, or whether there is a certain degree of alignment in the sample.

As mentioned before, the desired molecule conformation for a PVDF nanofiber is the β-phase configuration which enhances the piezoelectric response of the material. Performing a Fourier Transform Infrared Spectroscopy is a fast characterization test that can be done to determine the phase configurations of the sample in question. According to Mandal *et al* (2012) [49], when analyzing the absorbance of wavelength for a PVDF samples, the first three phases (α, β, and γ) can be seen in different proportions; the greater the peak, the greater the concentration of that phase. The usual frequency or wavenumber that the test runs is between 3000 to 500 cm^{-1}. Mandal *et. al.* reports that the α-phase peaks in the absorbance vs. wavenumber data can be found at frequencies close to 1212, 976, 764, 615, and 531 cm^{-1}. The β-phase can be found around 1275 (most predominant) and 445 cm^{-1}, with a dual signature shared with the γ-phase in frequencies around 841 and 510 cm^{-1}. The predominant signature frequency for γ-phase is 1233 cm^{-1}. Changes in temperature, mechanical elongation, and doping of other composites have shown to alter the magnitude and/or shift the frequency at which these phases are found. As reported by Garain *et al* (2014) [26, 27], the addition of Cerium-complexes to the

production of PVDF films almost erased any trace of α-phase present while increasing the magnitude of the β-phase configuration.

Table 5. Summary of PVDF conformation phases [27]	
Phase	Wavenumber (cm^{-1})
α-phase	1212, 976, 764, 615, 531
β-phase	1275, 445
γ-phase	1233
β- and γ-phase	841, 510

To determine the degree of crystallinity present, Differential Scanning Calorimetry tests can be performed for PVDF samples. Lanceros-Mendez *et al* (2001) [43] showed that for PVDF films with predominant β-phase configuration, there was only one endothermic peak between 150 and 160 °C which corresponds to crystal melting. The degree of crystallinity was measured as the ratio between the melting enthalpy of the of the material tested (ΔH_m) and the theoretical melting enthalpy of the totally crystalline material (ΔH_0=104.50 J/g for PVDF). In a study by Salimi *et al* (2003) it was shown that a higher melting temperature corresponded to a thicker crystalline lamella [63, 64].

Thermogravimetric Analysis which measures weight change as a function of temperature is also commonly used to fully characterize developed systems. The number of steps present in a TGA graph correspond to a compound from the material that degraded at that temperature. One step corresponds to a homogenous material while many steps relates to material made of many

different compounds such as alloys or composites. A shift in thermal degradation correlates to a change in the thermal stability of the material as reported by Achaby *et al* (2012) [1].

2.7-Nanogenerators/Harvesters

One of the main uses for PVDF films and fibers is in energy harvesting applications. Due to PVDF's sensitivity and chemical resistance, films and fibers made with this material respond to vibrations from different sources, for example sound or body movement. When correctly adapted for such application, the film or fiber mat can produce enough usable voltage by harvesting the motion of the system; whether it would be sounds waves coming from a speaker, or mechanical motion of a person walking. An efficient energy harvester is one with increased sensitivity. Hillenbrand *et al* (2010) [34] defines the sensitivity as the output voltage of electric response divided by the input force. If the harvester can sense small fluctuations in motion of a system and is able to harvest that and transform it into a usable amount of electric energy the harvester is said to have high sensitivity.

One of the principal aspects for producing an efficient energy harvester or generator is that the PVDF material, whether film or fiber, should be poled. Poling usually takes place by exposing the PVDF sample to a high voltage electric field which will reorient the dipoles in the PVDF making it more piezoelectric, thus increasing the response as seen by McKinney *et al* (1980) [51]. Other ways for poling include doping of other elements that will enhance the β-phase conformation as observed by Garain *et al* (2015) [27], as well as mechanical stretching of the PVDF fibers as reported by Vazquez *et al* (2012) [73].

The piezoelectric charge constants of PVDF also play an important role in the development of nanogenerators. With increasing poling, the piezoelectric constants should

change as to increase the piezoelectric response. Ting *et al* (2013) [70] characterized the piezoelectric constant d_{33} using a D33 meter Sinocera model YE2730. The input force and the output voltage were analyzed using a Dynamic Signal Analyzer PCB Piezotronics 086E80. Ting reports that the films that were poled showed an increased in the β-phase as confirmed by FTIR and DSC analysis. This increased in β-phase correlated to the increase in voltage response.

Other nanogenerator was developed by Pi *et al* (2014) [58]. This flexible nanogenerator was made of a PVDF-TrFE thin film deposited on a polyimide substrate with a gold electrode and a silicon oxide layer. This 6.5 μm thick film demonstrated to have a predominantly β-phase according to FTIR results as well as XRD. This nanogenerator had mechanical strains applied periodically by stretching and releasing the sample. The electrical outputs were recorded during stretching and releasing. It was determined that with varying frequencies between 0.25 to 0.75 Hz of strain application, the voltage output increases with increasing frequency. Voltages as high as 7 Volts, and current around 58 nA were observed for a frequency of 0.75 Hz.

As opposed to a PVDF film for energy harvesting, Xin *et al* (2016) [77] developed a nanogenerator sensor with PVDF nanofibers doped with nanoclay fibers. Fibers were produced using electrospinning. Fibers were deposited on a nickel-copper plated polyester fabric and were later covered with another conductive fiber to create a sandwiched structure. The sample was then encased with one sided adhesive transparent visible tape. To test for piezoelectricity, the sample underwent a free vibration test on a cantilever. Voltages detected from these tests ranged between 0.78 to 2.76 V. This sensor showed promising applications in smart textiles for its ability to register the respiration and pulse of a person and produce a proportionate response.

Orientation of the nanofibers has proven to be a decisive factor in power generation. For aligned fibers, an extra poling step is required to align the dipoles in the direction of the fiber

alignment. According to Fang *et al* (2011) [21], randomly oriented electrospun fibers can be used as a nanogenerator just by sandwiching these between two metal foils. Characterization tests confirmed that the 140 μm thick PVDF nanofiber membrane had a high β-phase concentration. Repeated impact tests with varying impact frequency were performed to determine the output voltage. Upon impact, the compression and release of the fibers was accompanied by a positive and a negative pulse voltage respectively. It was found that reversing the connections of the electrodes would reverse the polarity of the voltage and current outputs. Under 1 Hz compressive impacts, the average output voltage was 0.43 Volts, while for a compressive impact of 10 Hz produced a voltage output up to 6.3 Volts. For frequencies of 1, 5 and 10 Hz, the initial impact speed was 6.8, 34 and 68 mm/s; these low initial speeds prove that energy can be harvested from motions by the human body. The output voltages can be as high as possible, but they need to be stored in order to be harvested and used later. Fang (2011) converted the voltage outputs into DC signals using a full wave rectifier bridge. Under an impact frequency of 5 Hz, it took 2 min to charge a 2.2 μF capacitor to over 3 Volts. To light up a commercial LED, it took 30 min to charge the needed 33 μF capacitor.

2.8-Enhancing the nanogenerators

2.8.1-Doping with Salts

As seen already, nanogenerators are a viable way to harvest mechanical motion and converting it into usable electrical energy; the more sensitive the nanogenerator the lesser the force needed for it to respond. One way for enhancing the response is by doping the PVDF with composites that will increase the β-phase and make the fibers or film more conductive.

Self-poling of fibers can be obtained by incorporating fillers such as metal nanoparticles, metal oxides, metal salts, blending with polymers consisting of carbonyl groups, ceramics, and carbon derived products. An example of this research is performed by Hoque *et al* (2017) [38]. They produced a PVDF film based piezoelectric nanogenerator doped with Er^{3+} and Fe^{3+}; the films were referred to as EPENG for the one with Er^{3+}/PVDF and IPENG for the one with Fe^{3+}/PVDF. Studies have been done regarding the effect of rare-earth salts (R^{3+} cations) on the dielectric properties and crystalline structure of PVDF. The addition of the salts leads to vanishing peaks of α and γ crystals under XRD, while it increases the magnitude of the peak at $2\theta=20.5°$ confirming the presence of β-phase crystals. The fraction of β-phase content increases with loading concentration of each salt (5wt.% of $ErCl_3 \cdot 6H_2O$ and 10wt.% of $Fe(NO_3)_3 \cdot 9H_2O$). Further increase in concentration hinders the formation of the β-phase. The films with the highest concentration of β crystals were selected for voltage testing; the films were placed in between 2 electrodes and were given continuous finger compressions producing a positive open-circuit voltage of 115 Volts approximately, with a short-circuit current of 32μA for the EPENG film and 75 Volts with a current of 17μA for IPENG. It was determined that the presence of salt molecules trigger the piezoelectric β-phase formation by strong electrostatic interactions between the water molecules of salts and the negative $-CF_2$ dipoles of PVDF via formation of Hydrogen bonds. The study reported that the EPENG and IPENG were able to light up 54 and 42 commercially available blue LEDS connected in parallel, and 37 and 15 in series. Likewise, using a bridge rectifier, and with cyclic finger compressions on the films, the EPENG and IPENG were able to charge a 1μF capacitor to 3.8 Volts in 18 seconds, and 2.6 Volts in 22 seconds respectively.

2.8.2-Graphene composites

To improve the performance of the nanogenerators, researchers have proposed to use different carbon-based materials, such as carbon nanotubes (CNT), carbon black (CB), and graphene to alter the polymer microstructure and promote piezoelectricity. Amongst these, graphene has been deeply studied due to its flexibility, high aspect ratio, large specific surface area, excellent mechanical strength, and good thermal and electrical conductivities. According to Abolhasani *et al* (2017) [2], the addition of graphene to PVDF can induce nucleation of the piezoelectric β-phase.

Garain *et al* (2016) developed a in situ poled Ce^{3+}-doped electrospun PVDF/graphene composite nanofibers for ultrasensitive acoustic nanogenerator. They demonstrated the effects of in situ poled ultrasensitive pressure sensor via electrospinning process, where few monolayers of graphene sheets are encapsulated in the Ce^{3+}-doped PVDF matrix. Through XRD it was demonstrated that the electrospun fibers doped with Ce^{3+} diminished the presence of α-characteristic diffractions, while the β- and γ-phase appeared. Also, the addition of graphene corresponded to an enhance on the concentration β crystals. Analyzing the morphology of the produced fibers, the SEM images showed a smooth surface; no mass or lumps (agglomerates) of graphene are seen on any of the images. Due to the carbon-based structure of graphene and the PVDF polymer, the graphene was well dispersed within the polymer matrix. Experiments show that the nanogenerators developed were able to sense small pressure values such as 2 Pa. It is also reported that pressing the nanogenerator with an approximate frequency of 4Hz and a force of 8N (external pressure of 6.6 kPa)—which is comparable to the peak plantar pressure of a human finger touch—the nanogenerator produced an open-circuit voltage of 11 Volts and a current density of 6 nA/cm^2. It was also reported that under a sound pressure level (SPL) of 88

dB, the nanogenerator produce a voltage of 3 Volts, while for other sounds such as a piano, guitar, or violin solo of same SPL, the voltage generated was up to 1.2 Volts. On a side note, the ultra-sensitivity of the nanogenerator makes it useful to map input voice or speech signal. Using an SPL of 88 dB and connected to a bridge rectifier, the nanogenerator was able to light up three commercially available LEDs connected in series, as well as individually connected capacitors of 1, 2.2, and 4.7 μF. Since the nanogenerator demonstrates to be useful for a wide variety of applications, tests were conducted to see the efficiency of the nanogenerator as a wind energy harvester. Attaching the nanogenerator to the end of a table, and with winds blowing at speeds from 0.5 m/s to 8 m/s, the voltages produced increase from 0.6 Volts to approximately 3.2 Volts. With velocities higher than the ones previously mentioned, the voltage response is significantly reduced, and almost negligible at speeds of 15 m/s.

2.8.3-Polypyrrole doping and coating

Another method for enhancing the piezoelectricity of PVDF is by doping or coating the nanogenerator with conductive polymers. According to recent studies, Polypyrrole (PPy) is a conductive polymer that seems promising for commercial applications in substituting some metal conductors or semiconductors. PPy has shown to have good environmental stability, facile synthesis and higher conductivity than many other conductive polymers according to Chougule *et al* (1999) [16]. PPy can be used for biosensors, gas sensors, wires, microactuators, antielectrostatic coatings, polymeric batteries, etc. PPy can be easily prepared by either an oxidatively chemical or electrochemical polymerization of pyrrole. One disadvantage of this material is that it is insoluble and infusible in many organic solvents; consequently, it restricts processing procedures.

Polypyrrole has been used in the development of supercapacitors. In general, Pseudocapacitors with electrodes made up of metal oxide/hydroxides and conducting polymers, employ the oxidation/reduction mechanism, which occurs within the electrode materials as studied by Qu *et al* (2011) [59] and Ghosh *et al* (2013) [29]. As mentioned before, graphene's hexagonal structure, and its high electron motility and low resistivity makes it a great material for conductive applications. Similarly, PPy is an attractive pseudocapacitor because of its properties previously mentioned, but moreover because of its mechanical flexibility due to the demand for flexible supercapacitors, as reported by Snook *et al* (2011) [67]. To prepare a supercapacitor, Chee *et al* (2014) [13] prepared a Polypyrrole/Graphene Oxide/Zinc Oxide nanocomposite. The PPy/GO/ZnO nanocomposite was deposited on a nickel foam which served as the working electrode, with a platinum rod as the counter electrode. The results demonstrated that the ternary nanocomposite exhibited a specific capacitance of 123.8 F/g at 1 A/g, with a typical pseudo-rectangular CV shape at a two-electrode configuration which indicates an ideal charge/discharge behavior. This model was able to light up an LED even after it was bent, proving the concept of a flexible storage device.

Table 6. Summary of Voltages from Literature				
Source	**Material**	**Type**	**Testing method**	**Results**
[21] Fang et al (2011)	PVDF	Electrospun fibers	Compressive impacts (1-10 Hz)	0.43-6.3 V
[70] Ting et al (2013)	PVDF-Indium Tin Oxide	Film	Mechanical loading (0.24, 0.56N)	0.15-0.25V
[56] Nilsson et al (2013)	PVDF-HDPE-Carbon Black	Film	Mechanical loading (0.05 N)	4 V
[77] Xin et al (2015)	PVDF-nanoclays (randomly oriented fibers)	Electrospun fibers	Free vibration damping	1.65 V
	PVDF-nanoclays (oriented fibers)	Electrospun fibers	Free vibration damping	2.76 V
[2] Abolhasani et al (2016)	PVDF/Graphene	Electrospun fibers	Compressive impacts (0.2 MPa, 1Hz)	3.8-7.9 V
[19] Dong et al (2017)	PVDF-PDMS-PI	Composite film	Small body movements	4 V
[66] Sharma et al (2012)	PVDF-TrFE	Film	Pressure loading (20-300 mmHg)	40mV
[58] Pi et al (2014)	PVDF-TrFE	Film	Compressive impacts (0.25-0.75 Hz)	3-7 V
[76] Wang et al (2016)	PVDF-TrFE-PDMS/MWCNT	Electrospun fibers	Compressive impacts (5 N, 1-4 Hz)	1.5-2.5 V
[14] Chen et al (2016)	Ag doped PVDF-TrFE	Composite film	mechanical loading	48 mV
[27] Garain et al (2015)	Ce+3-Doped PVDF (1 wt.%)	Film	Finger tapping	1.8 V
	Ce+3-Doped PVDF (0.06 wt. %)	Film	Finger tapping	32 V
[26] Garain et al (2016)	Ce+3-Doped PVDF/Graphene	Electrospun fibers	Finger tapping	11 V
	Ce+3-Doped PVDF	Electrospun fibers	Finger tapping	4.5 V

[38] Hoque et al (2017)	Er+3 doped PVDF	Film	Finger tapping	115 V
	Fe+3 doped PVDF	Film	Finger tapping	75 V

Table 6 shows the summary of the voltages produced by the PVDF fibers and films. Here, the specimens tested are compared; as seen, the results range from 0.43V to 115V. Considering the maximum and minimum results as outliers, there common range of voltage results fall between 3-8V. From the literatures study it can be observed how the PVDF in fiber form tend to produce higher voltage results. As of this date, there is no literature covering Forcespun PVDF nanofibers with graphene and Cerium-complexes doping, with a PPy coating and mechanical poling.

CHAPTER III

EXPERIMENTAL TECHNIQUES

3.1. Forcespinning

Fiber production has been improved by Forcespinning®. Production yield is about 600 times greater than Electrospinning. This method of production uses centrifugal forces to make a polymer viscous solution into a polymer nanofiber as studied by Padron *et al* (2012) [57].

When a polymer solution is place inside the spinneret, the rotating part inside the Forcespinning machine, as the revolutions per minute increase, the viscous solution moves towards the orifices on each side of the spinneret. As the polymer exits the orifices, it forms a droplet that extends and forms a polymer jet as the solvent evaporates. This jet elongates as it rotates and once it is long enough it will be deposited on the metal collectors inside the machine. Key factors for fiber creation are evaporation rate, viscosity of solution, rotating speed, distance from collector, humidity and temperature of the room, temperature of solution, and solvents used.

Once fibers are collected, they form a donut shape around the metal collectors. Collection will vary depending on the application; for example, if fiber alignment is important, collection of fibers from collectors will be done by removing all the fibers in one direction. To improve fiber elongation, an external rotating cylinder is placed inside the Forcespinning machine. The

cylinder is operated by a 12V DC motor and powered by a power supply. As the fibers are being formed and are rotated, the cylinder is rotating and trapping all the fibers; as it rotates, the fibers stretch once more, and their diameter is reduced all while keeping alignment and fiber orientation.

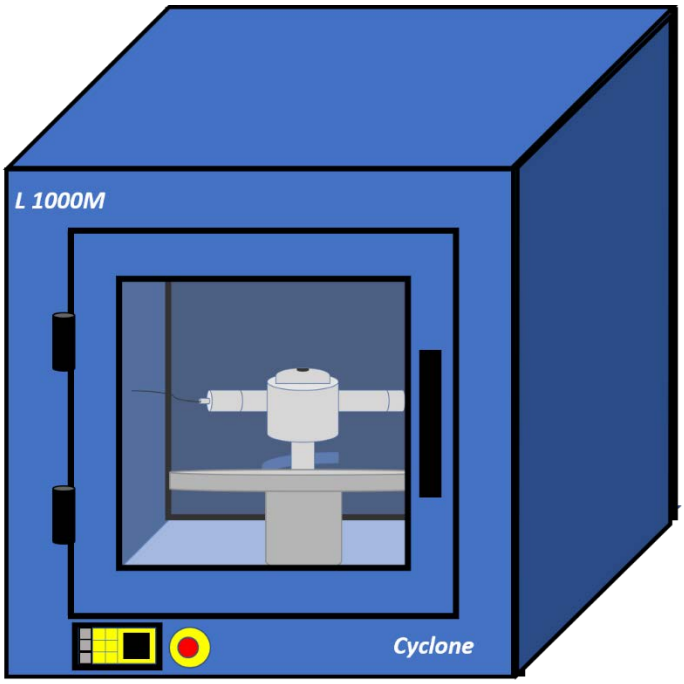

Figure 1: Forcespinning® Machine Cyclone

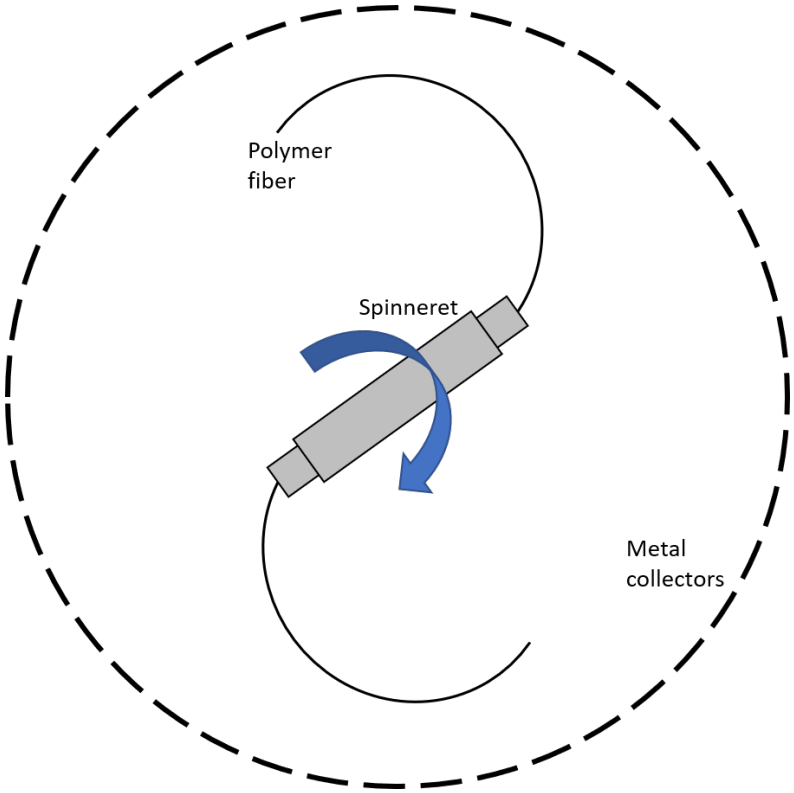

Figure 2: Fiber jet coming out of the spinneret and moving towards metal collectors

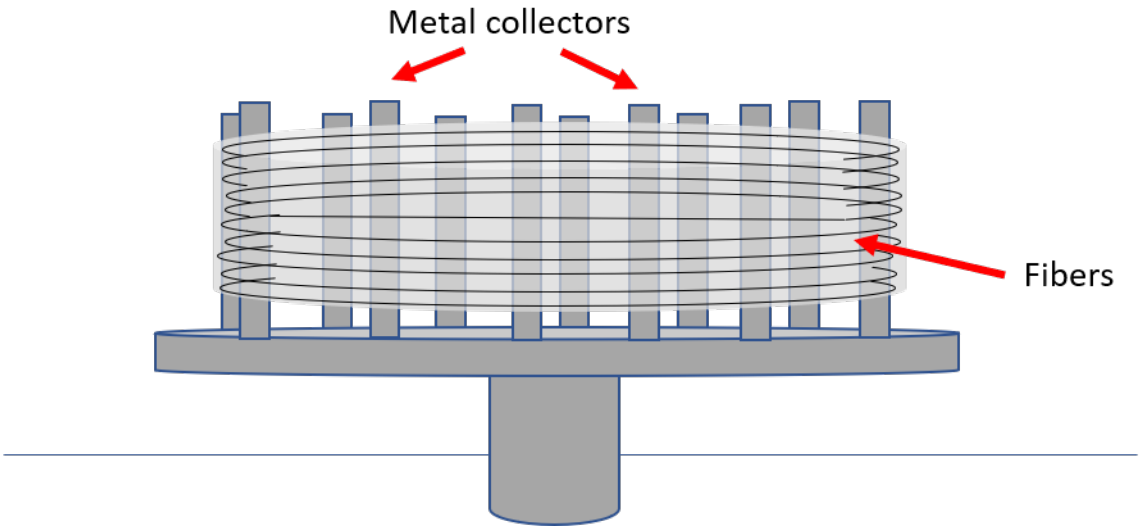

Figure 3: Fibers deposited over metal collectors after Forcespinning®

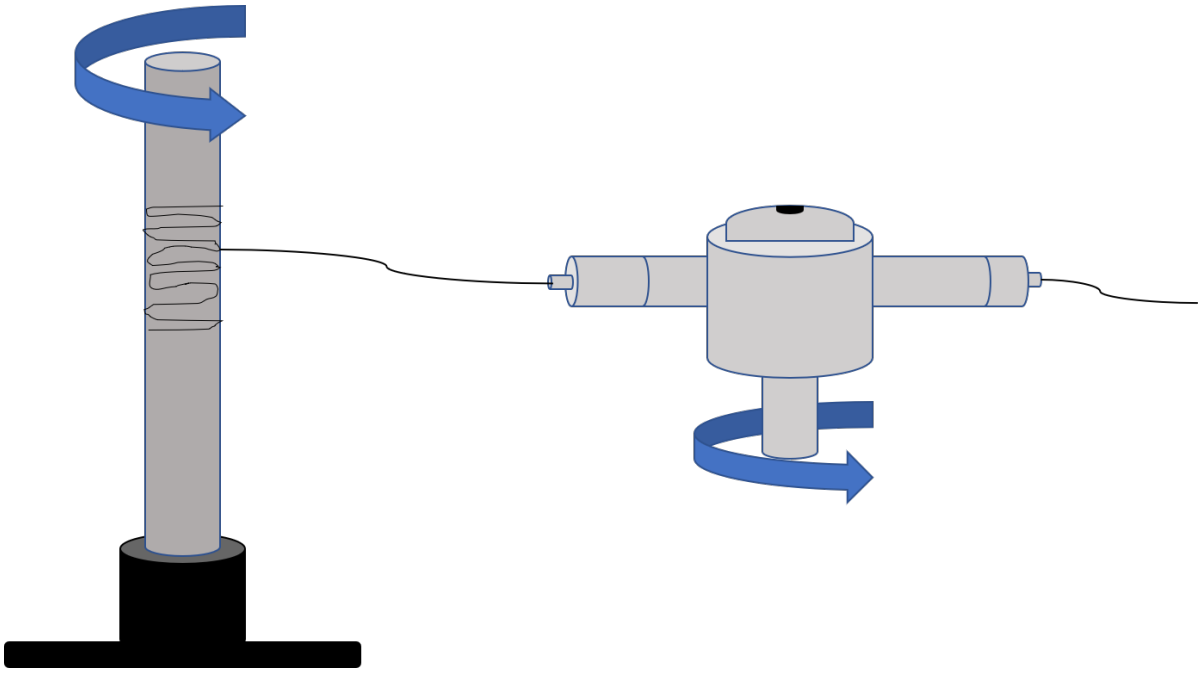

Figure 4: Cylindrical rotating collector elongation and catching fiber form spinneret

3.2. Characterization

There are different methods that can be applied to characterize a material in different aspects; thermal analysis can be performed to determine the thermal properties of a sample; infrared spectroscopy is used to determine the "fingerprint" information of the elements present in a material, while X-Ray Diffraction is used to determine the internal structure of a sample. The techniques presented for this project include TGA, DSC, FTIR, XRD, SEM, and Piezoelectricity testing.

3.2.1. Scanning Electron Microscopy Analysis

At plain sight the physical characteristics of the nanofibers are not visible. With the help of a Scanning Electron Microscope fiber samples can be observed with detail precision on the

micron and even nano level. Characteristics such as morphology of the samples, fiber diameter, compounds present, and alignment of the fibers can be observed using Electron Microscopy.

The SEM has five main components for basic functioning; source of electrons, the column where electrons travel, electron detector, sample chamber, and computer display. Electrons are produced at the top of the column in the electron gun. They are then accelerated using lenses and apertures producing a focused beam of electrons that hits the sample in the chamber below all in vacuum conditions. The SEM produces images by scanning the surface of the sample with a high-energy beam of electrons. When the electrons hit the samples, they cause electrons from the sample to be displaced—secondary electrons, and backscattered electrons, as well as creating X-Rays characteristic to the elements present. These signals, secondary and backscattered electrons, are then collected by a detector and form an image on the computer.

The resolution of the sample image can be altered depending on different factors such as electron spot size, aperture diameter, magnitude of voltage applied, and conductivity of sample; for samples that are not conductive, they are sputtered with gold nanoparticles to help the bouncing of electrons which will be detected and will form the image. Other factors affecting the resolution of the microscope are the lenses and the wavelength of light used. A disadvantage to light microscopes is their limited resolution power since white light has a wavelength between 400-700nm, thus samples smaller than 400nm will not be visible. Since electrons have shorter wavelengths, this enables a better magnification and resolution that allows for imaging samples in the low end of the nano scale.

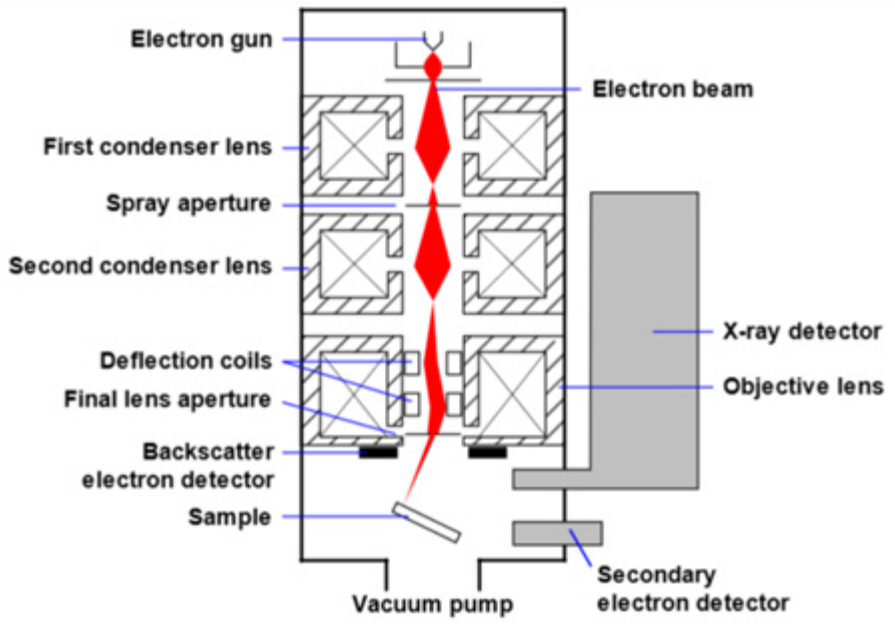

Figure 5: Schematic of Scanning Electron Microscope [65]

3.2.2. Spectroscopy Analysis: Fourier Transform Infrared Spectrum

Spectroscopy is the technique of splitting light, or electromagnetic radiation, into its constituents wavelengths—like how a prism divides white light into colors. Being a broad field, spectroscopy techniques are divided into sub-disciplines according to the implementation. Not only is electromagnetic radiation observed, other sources such as de Broglie waves and radiated acoustic waves can be analyzed. Techniques such as Fourier Transform Infrared Spectrum (FTIR), X-Ray Diffraction (XRD), Raman Spectroscopy, and Nuclear Magnetic Resonance (NMR) are found under the spectroscopy umbrella.

Fourier Transform Infrared Spectroscopy or FTIR, is one of the preferred methods for detection of molecules present in a polymeric or organic sample. When a sample needs to be tested, a controlled amount of Infrared radiation is applied to the sample; some radiation is

absorbed, while some passes right through (transmitted) depending on the material. The resulting data is a spectrum signal that represents the molecular 'fingerprint' of the sample. Different materials have different wavelengths were energy is absorbed or transmitted, thus many materials and their different phases and conformations can be identified.

Interferometry is used to record information about the material placed in the IR beam, while the Fourier Transform results are analyzed to identify and quantify the material present. Using FITR, the phases present for a PVDF nanofiber can be determined as well as their concentration and how they vary as more dopants are added. Using Equation (1), Beer-Lambert's Law, the beta-phase formation of the PVDF fibers can be calculated. The values used for A_α and A_β correspond to the intensities of the sample being analyzed at 530 cm^{-1} and 840 cm^{-1} respectively. [49]

$$F(\beta) = \frac{A_\beta}{1.26A_\alpha + A_\beta} * 100\% \qquad \text{Eq. (1)}$$

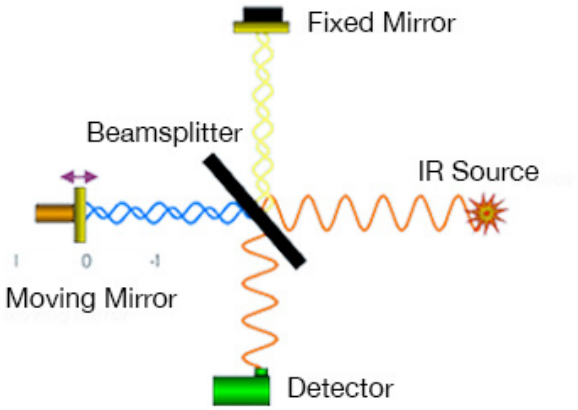

Figure 6: Schematic of Fourier Transform Infrared functioning [23]

3.3 Piezoelectric Testing

3.3.1 PVDR Pro

As mentioned before, piezoelectricity is the effect of producing an electrical response from a mechanical input and vice versa. In this case, applying a certain force, causing a recoverable deformation to a piezoelectric material, will produce a proportional electrical response. The following equation relates the input force to the voltage produced.

$$V = \frac{d_{ij}}{\varepsilon_{ij}} * \frac{F}{At} \qquad \text{Eq. (2)}$$

V is the voltage output, F is the force applied, A represents the area where the force is applied, and t is the thickness of the sample. Parameter 'd' corresponds to the piezoelectric activity of the sample when 1 Pa of pressure is applied along the "j" direction resulting in an electrical value measurement along the "i" direction, while 'ε' indicates the permittivity of the material. Equation (2) can be then further simplified resulting in Equation (3). [11]

$$V = g_{33} * \frac{\sigma}{t} \qquad \text{Eq. (3)}$$

3.3.2 Bridge Rectifier

In order to harvest energy from motion, a signal converter is needed. Harmonic mechanical oscillations that power the piezoelectric sensor for energy harvesting creates a harmonic voltage response—a positive and negative voltage; however, to power an electronic device, only the positive side of the signal is taken into consideration, thus only powering partially the device. To efficiently power an electronic device, both positive and negative parts of

the AC signal should be converted to DC. A bridge rectifier is a circuit that converts an AC signal into a DC signal. The circuit consists of an AC power source, 4 equal diodes connected as seen in the diagram below, a load which is an element that add resistance to the circuit such as an LED or a resistor, and a capacitor.

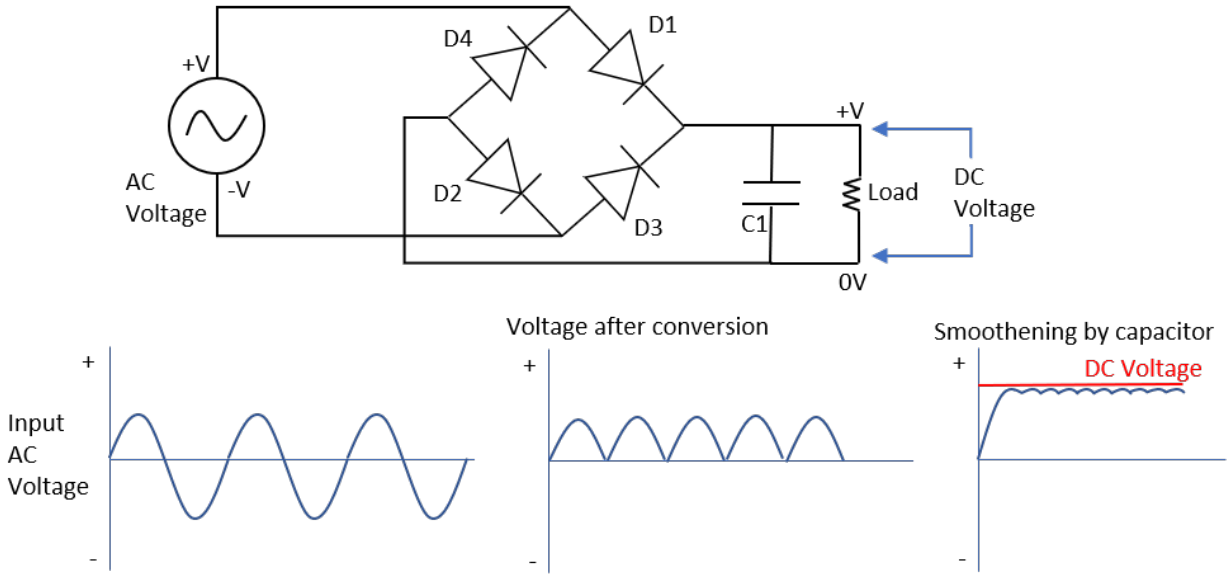

Figure 7: Schematic of Bridge Rectifier Circuit and signal conversion

Since diodes only allow for current to flow in one direction, both positive and negative voltage arrives to the load as a positive DC signal. Starting at the input with the positive voltage peak, current will flow towards diode D1, as mentioned before, current will not flow through diode D4 because the path is “blocked” or “closed”, nor it will enter D3 for the same reason after flowing through D1. Current will then flow towards the capacitor and the load in parallel and then flow back an enter D2. After diode D2 the current returns to the voltage source. Continuing with the negative voltage peak, current will flow backwards towards D3; it will get to the capacitor and the load as a positive voltage and will flow back towards D4 returning to the voltage sources. Both loops turned positive and negative AC signals into DC.

The purpose of the capacitor is to make the signal smoother making it resemble more a DC signal; the higher the capacitance, the smoother the signal gets.

3.4 Thermal Analysis

3.4.1 Thermogravimetric Analysis

A method for characterizing the compounds present in a sample is using Thermogravimetric Analysis. Thermogravimetric Analysis or TGA, is a method of thermal analysis which examines the mass changes of a sample as a function of temperature or time. One method for TGA testing is by heating a sample at a constant rate until a desired temperature is reached; the other method is by heating a sample at constant temperature for a specified period. The results are presented in changes in weight percentage vs temperature or time. The changes of mass of the sample are due to several reasons such as desorption, absorption, sublimation, vaporization, oxidation, reduction and decomposition. Since different compounds have different thermal properties, for a sample with different materials present, a drop in the weight is expected to appear at different temperatures. The number of shoulders or drops present on the graph correlate to the number of different compounds present in the sample and the temperature at which they degrade. For this experiment, TGA was used to test the thermal stability of the nanofibers and observe the effects of dopants on the degradation temperature of the samples.

The parameters used for this experiment were the following: a 10mg sample from each fiber was taken and placed inside the Texas Instruments TGA Q500 with a heating rate of 10 °C/min starting at room temperature 30 °C and heated until 800 °C. Results were gather as text file and plotted in graphs.

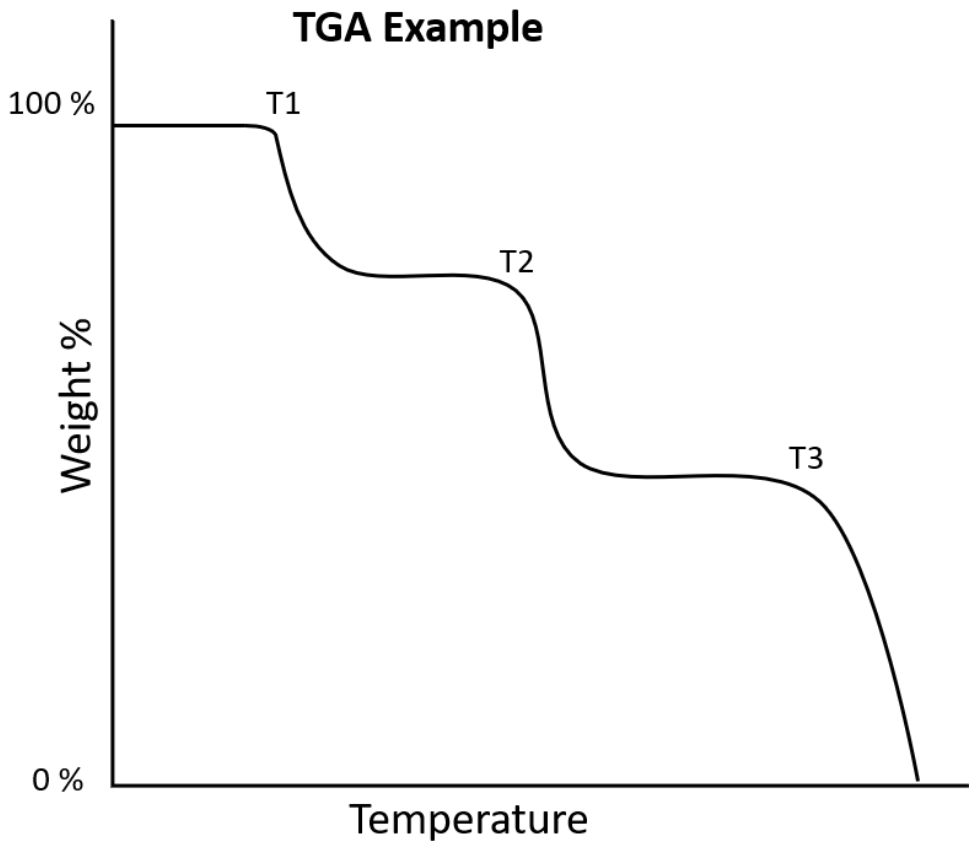

Figure 8: TGA example graph showing degradation of 3 different compounds in a sample

3.4.2 Differential Scanning Calorimetry

Differential Scanning Calorimetry (DSC) is a technique used for studying the thermal transitions polymers. It is useful in determining whether a polymer is amorphous or crystalline and shows what kind of reactions are happening on the material as the temperature changes. DSC works by comparing the energy absorbed or released from the sample at a given temperature in relation to a reference point. Two hermetically sealed, metal pans are used, one empty and one with the sample inside and both are heated at a constant rate until a desired temperature; unlike TGA which heats up the samples beyond their degradation point, DSC heats up the samples in the temperature range just before degradation occurs. DSC is often seen as the technique used for

finding the thermal fingerprint of a material. Heating at different rates may affect the transitions of certain materials, making them take longer or faster time to melt or crystallized. Cooling may also be performed with DSC; by cooling the sample at a certain rate, the glass transition phase of a material can be obtained if the sample has a glass transition well below that of room temperature. The data is presented with Energy in mW or mW/g on the dependent y-axis and temperature on the independent x-axis. Whenever energy is absorbed (endothermic reaction) or released (exothermic reaction) by the sample, peaks appear on the graph; the direction may vary with peaks being exothermic and valleys endothermic or vice versa, however it is always specified on the graph in which direction the energy flows. Most of the time valleys represent endothermic reactions such as melting, while peaks represent exothermic reactions like crystallization for thermoplastic materials only. Shoulders present on the graph correspond to the transition temperature of the sample, while some small peaks may be due to curing of a thermoset sample. DSC test are done in cycles usually; heating and cooling cycles. By doing at least two equal cycles the thermal history of the material can be erased. In the first cycle the data will show if there is any volatile present or any transition. By the second cycle, the volatiles might have been evaporated and what remains is mostly pure material.

DSC is useful in the determination of the crystallinity content of a semi-crystalline thermoplastic material. The degree of crystallinity for a polymer can be calculated using the following equation.

$$\chi = \frac{\Delta H_F}{\Delta H_F^0} * 100\% \qquad \text{Eq. (4)}$$

'χ' represents the degree of crystallinity of a sample, ΔH_f is the heat of fusion of the material in J/g, or the enthalpy of the melting peak, and ΔH_f^0 is the theoretical heat of fusion for a 100% crystalline sample of the material. For PVDF, the theoretical heat of fusion is approximately 103-105 J/g [73].

For this experiment, two cycles of heating and cooling from 30-250 °C were used for all the samples.

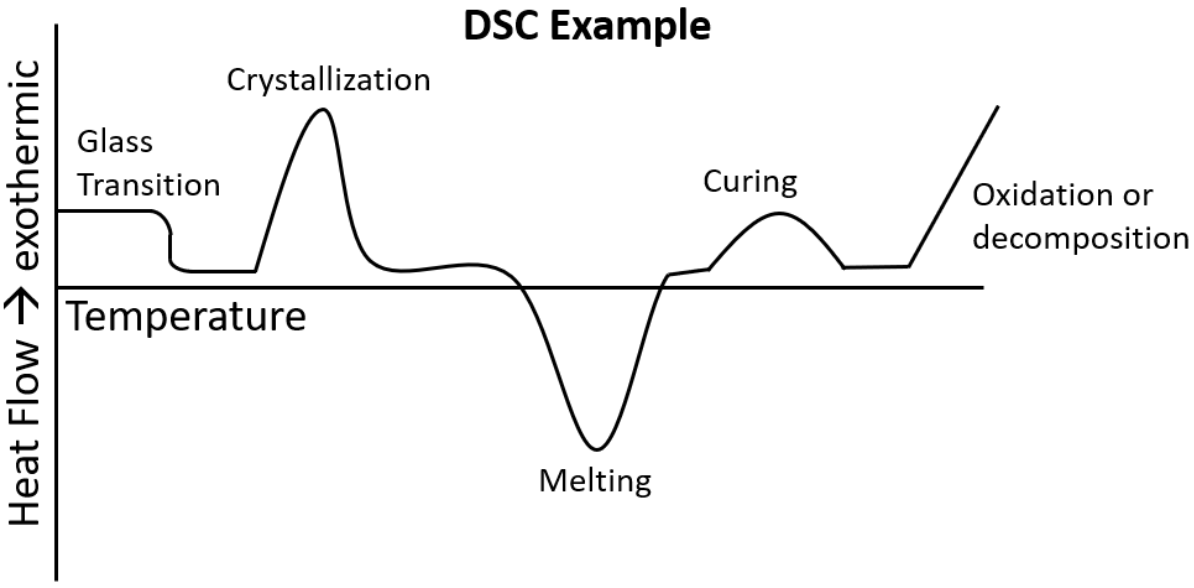

Figure 9: DSC example graph showing important peaks and transitions found in DSC data

CHAPTER IV

METHODOLOGY

The production of nanofiber-based membranes involves different steps: (1) solution preparation, (2) solution spinning, and (3) collection of developed fibers. The thermo-physical, electrical, and piezoelectric response of the developed systems is then analyzed. All processes are performed in a controlled environment following proper safety measures.

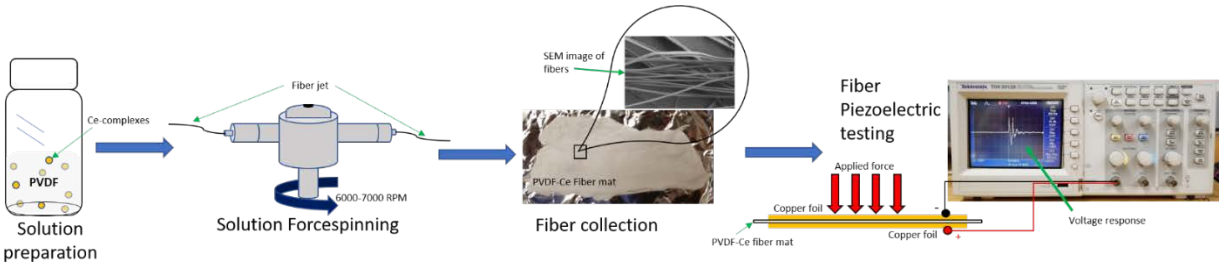

Figure 10: Graphical description of processing and testing methodology

4.1 Solution Preparation

The materials needed for solution preparation are the following. All materials were obtained from Sigma Aldrich with exception of the PVDF powder.

Solvents: N-N-dimethylacetamide (*DMA*), Acetone.

Polymer: PVDF KYNAR 741from Arkema, Inc.

Dopants: Ammonium Cerium (IV) Sulfate Dihydrate *(CAS) (Ce* $(NH_4)_4(SO_4)_4 \cdot 2H_2O$*, USA);* Cerium (III) Nitrate Hexahydrate (CAS) *(Ce* $(NO_3)_3 \cdot 6H_2O$*, USA),)*; Graphene powder;

Polypyrrole, doped, conductivity 30 S/cm (bulk), extent of labeling: 20 wt. % loading, composite with carbon black; 5 wt.% PPy dispersion in water.

4.1.1 Control Solution

Different solutions varying the concentration of PVDF were prepared and it was observed that the optimum concentration based on synergy among output and fiber diameter was 22 wt.% PVDF solution in a 1:1 ratio of DMA and Acetone as solvents. This concentration will serve as control throughout the experiment. To prepare a 5g solution, 1.1g of PVDF powder was weighted on a four-digit, electronic scale and placed inside a 20mL glass vial. A magnetic stirrer was places inside the vial to mix the solution when solvents were added.

1.95g of DMA were measured by calculating the mass of the liquid volume of the solvent using its density, 0.94 cm^3/g. Once the desired amount was reached, the solvent was deposited in a second 20mL glass vial. 1.95g of acetone were measured in a similar manner and places in a third glass vial. Both solvents were poured onto the vial with the PVDF powder; solution was then taken to a preheated oil bath and was left mixing for 60 to 90 min between 70-75 °C.

4.1.2 Cerium doped PVDF solution

Six different doped solutions were prepared for this experiment involving Cerium-complexes. For each Cerium-complex, Cerium Nitrate and Cerium Sulfate, three solutions with varying weight percentage of the dopant were created. Weights of dopants were 2.5, 5, and 7.5 wt.% for both dopants. Solution preparation follows the same procedure as the control, but before pouring solvents on the powder, 0.025g, 0.05g, and 0.075g of the corresponding Cerium-complex was added. In total 6 different doped solutions were prepared.

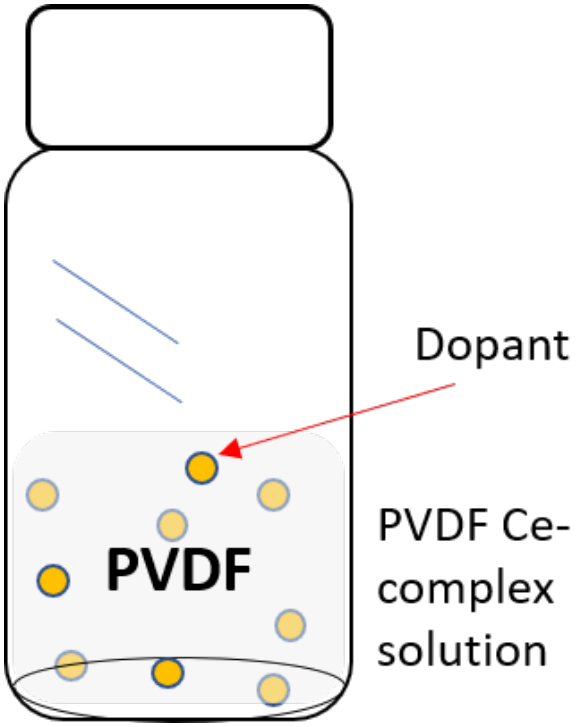

Figure 11: PVDF Ce-Complex solution in glass vial after preparation

4.1.3 Polypyrrole and Graphene doping

Two different doped solutions involving PPy and Graphene were prepared for this experiment. Procedure followed is the same as the control, but PPy and Graphene were added in different quantities. The dopant use for the PVDF-PPy solution was a Polypyrrole, doped, conductivity 30 S/cm, powder with 20 wt.% loading, composite carbon black. Doping for PVDF-PPy solution consisted of only 10 wt.%, or 0.1g. For the PVDF-Graphene solution, 5mg of Graphene powder were added as perceived to be the optimum concentration as seen from literature. [2]

4.2 Solution Spinning

Once the solution was stirred for around 90 minutes at 70-75 °C, the temperature of the oil bath was reduced to 50-55 °C enough to keep the solution warm and less viscous. Each 5g solution efficiently prepared yields 4-5mL worth of liquid solution for spinning. The machine used for Forcespinning® of the PVDF-X (nothing, CeN, CeS, PPy or Graphene) solution was the Cyclone L1000M from Fiberio Technology Corp. Spinning parameters used for the machine ranged between 6300-7000 RPM depending on the viscosity of the solution; more viscous solutions required higher RPM while less viscous used lower RPM.

For each round of spinning, 1.5-2mL of solution were injected into the metal spinneret inside the Cyclone using a 3mL syringe. For fibers to be formed, the exiting diameter from where the solution comes out on the spinneret must be small, thus 30G needles were used on each side of the spinneret as seen on the figure below.

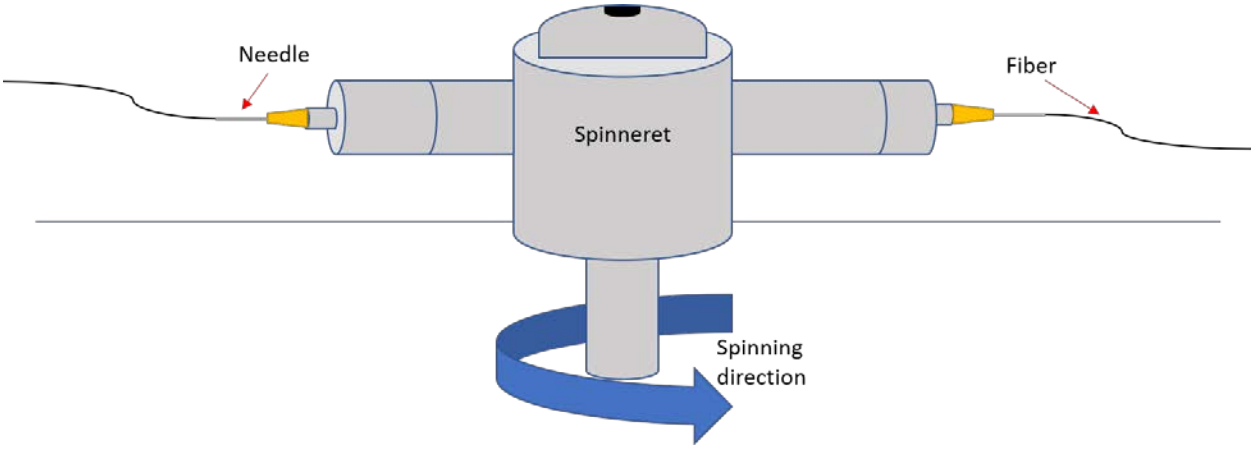

Figure 12: Schematic of fiber coming out of the needles in the spinneret

Eight rectangular metal stands, or metal collectors, wrapped in aluminum foil were placed inside the Cyclone before spinning evenly distributed; these metal collectors would catch the fibers as they come out the spinneret. Collectors distance from the spinneret fell between 8-11 inches depending on the solution's viscosity as well as the room's temperature and humidity—for optimum fiber production a room temperature between 68-72 °F and a humidity between 40-45% are desired. Solution was then spun at the desired RPM for 5-6 min per round. Once all the solution had come out the spinneret and the spinning time had concluded, fibers caught in the metal collectors were collected by rolling a cardboard cylinder wrapped in aluminum foil as to collect all the fibers maintaining the alignment and to avoid tearing them apart in sections. Fibers collected were laid flat on aluminum foil to create fiber mats.

4.3 Fiber PPy coating

To increase the conductivity of the PVDF nanofibers, they were coated with a highly conductive polymer, Polypyrrole. Two different Polypyrrole derivatives were used for coating, and eight different methods for coating were prepared. PVDF Neat, or pure PVDF, nanofiber mats were used to try all the coatings.

4.3.1 Method 1: Pure PPy coating

A 1x2 cm fiber mat was placed in a plastic weighing cup. Using a disposable pipet, 1 mL of 5 wt.% PPy dispersion in water was added on top of the fiber mat. Addition of PPy continued until fiber mat was covered in PPy droplets.

4.3.2 Method 2: PPy dilution in water

A 1x2 cm fiber mat was placed in a plastic weighing cup. One droplet of 5 wt.% PPy dispersion in water, 370mg, was diluted with 8-10mL of distilled water. PPy-water solution was

then added 1 mL at a time using a disposable pipet. Addition of PPy-water solution continued until fiber mat was covered in PPy diluted droplets.

4.3.3 Method 3: Iron-Nitrate/Water/PPY solution

To increase the solubility of PPy, a solution of 2.7 g of Iron (III) Nitrate-nonahydrate and 80 mL of water were mixed, and 0.25 mL of 5 wt.% PPy dispersion in water were added. A 1x2 cm nanofiber mat was placed inside Iron-PPy solution until the mat got wet. After wetting the mat, it was placed on a plastic weighing cup. PPy-water solution was added one droplet at a time to fiber mat until it was covered, then left to dry for 24 hours.

4.3.4 Method 4: Iron-Nitrate/Water/PPY solution with DMA and Acetone

Method 4 follows the same procedure of Method 3 just before addition of PPy-water solution to fiber mat. Varying amounts of 1:1 ratio of DMA and Acetone were prepared in glass vials. Concentrations of DMA and Acetone were 20, 30, 40, 50 and 60 wt.% as if used for a PVDF solution (usual concentration for 22wt.% PVDF solution is 78wt.% solvent). One droplet of the Iron-PPy solution was added to each DMA/Acetone vial. An 8-10mL of water with 370mg of 5 wt.% PPy dispersion in water solution was prepared. Fiber mats were then wetted by the Iron-PPy-DMA/Acetone solution and then covered with the PPy-water solution till fully covered, then left to dry for 24 hours.

4.3.5 Method 5: PPy-water/Ethanol solution

Method 5 resembles the procedure for Method 2. Ethanol was added to the PPy-water solution in different concentrations. Fibers were then wetted with PPy-water-ethanol solution until fully covered and left to dry for 24 hours.

4.3.6 Method 6: PPy-water solution and Ethanol coating

Method 6 resembles Method 2. Fiber mat was wetted with ethanol till fully covered, then it was covered with PPy-water solution until covered completely.

4.3.7 Method 7: Pure PPy with Ethanol coating

Method 7 resembles Method 1 in procedure, but in this method the fiber mat is wetted using ethanol droplets, and then applying the pure PPy (5 wt.% PPy dispersion in water solution) until fiber mat is fully covered.

4.3.8 Method 8: PPy with carbon black solution in water with Ethanol coating

A solution of Polypyrrole, doped, conductivity 30 S/cm (bulk), extent of labeling: 20 wt. % loading, composite with carbon black and water was prepared. 10mg of PPy were added to 8-10mL of distilled water and then stirred. Fiber mat was then wetted with ethanol and covered in PPy/carbon black-water solution till fully covered.

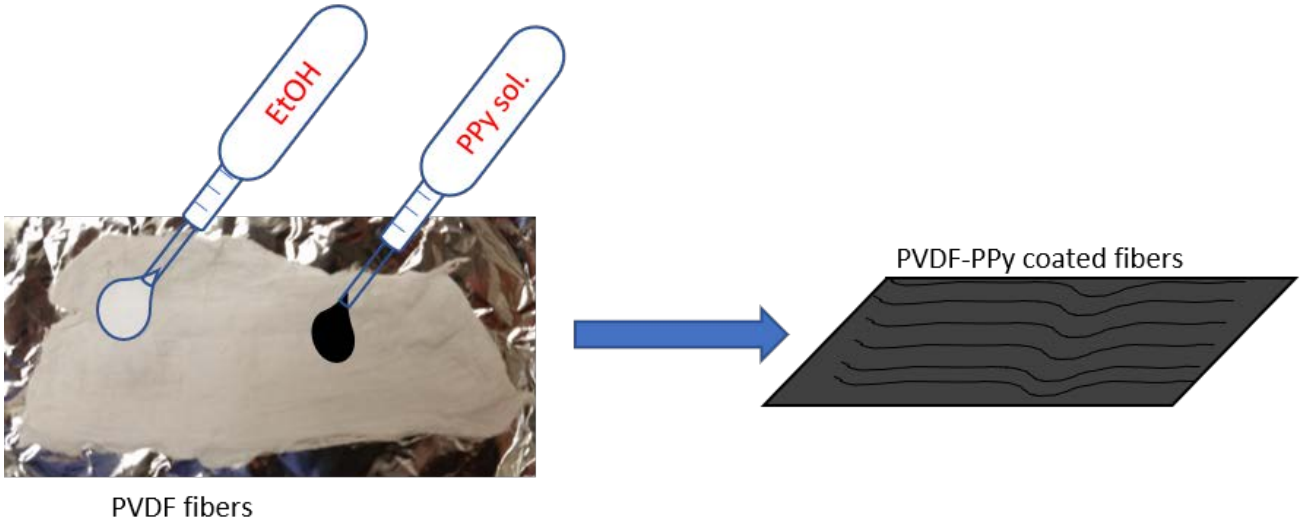

Figure 13: Graphical depiction of PPy fiber coating for Method 7 and 8

4.4 Piezoelectricity testing

To test for piezoelectricity on the nanofibers, the following set up was used. The PVDF fiber mats were set between two 5cm by 5cm copper foil plates working as electrodes and connected to a Tektronix TDS 1001 B Oscilloscope. A pneumatic cylinder stroked the specimen with an adjustable force measured using a load cell, with a frequency of 1.6 Hz and a pneumatic pressure of 30 psi. The piezoelectric response was recorded using the oscilloscope were the signals recorded were the minimum, maximum, and peak-to-peak voltages.

Figure 14: PVDR-Pro and Oscilloscope set up for piezoelectric testing

4.5 Characterization

4.5.1 SEM analysis

The morphology and average diameter of the fibers were analyzed using a Zeiss EVO LS10 Electron Microscope operated at 1-3kV.

4.5.2. Thermal Analysis: TGA

Thermogravimetric analysis was performed using a TGAQ-500 at a rate of 10 °C/min from room temperature to 1000 °C for 10mg of fiber sample.

4.5.3 Thermal Analysis: DSC

Differential Scanning Calorimetry was performed with a DSCQ-100. 5 mg of fiber sample was needed. Testing consisted of 2 heating and cooling cycles with isothermal segments. Starting from room temperature, 30 °C, the temperature increased at a rate of 10 °C/min till 250 °C; then it remained isothermal for 10 minutes and cooled down at 10 °C/min back to 30 °C, where once it reached the desired temperature it remained isothermal for another 10 minutes. Cycle 2 followed same procedure.

4.5.4 FTIR Spectrum Analysis

A 2x2 fiber mat was cut and placed inside the FTIR machine for testing. The crystalline β-phase of the fibers were determined using Fourier transform infrared spectroscopy (FTIR), Thermo Nicolet Nexus^{TM} 470 FT-IRESP.

CHAPTER V

RESULTS AND DISCUSSION

5.1 Fiber production

5.1.1 SEM Analysis

After fibers were spun, and fiber mats were collected, the sample were sputtered with gold to increase surface conductivity for successful electron microscopy analysis. All samples, aligned, misaligned, with graphene, and doped with Polypyrrole were analyzed for fiber diameter determination and fiber surface morphology. The following images presented were taken using the Zeiss EVO LS10 Electron Microscope, with a charged voltage of 1kV, and a SE2 signal lens.

Figure 15 shows an SEM image for a Neat PVDF or control fibers, and other PVDF fibers with Cerium-complexes. As seen on Figure 15.a, some fibers are randomly oriented while others are oriented in the same direction; this is due to the forces exerted on the fibers while spinning as well as the orientation of the fibers while being manually collected.

Figure 15.b shows a section of the PVDF control fibers showing fiber alignment. It can be seen how these fibers show a smooth surface morphology, meaning there are no rough patches or beads in the fibers. The average fiber diameter for the control sample is 0.9 μm, with range of 0.8-1 μm.

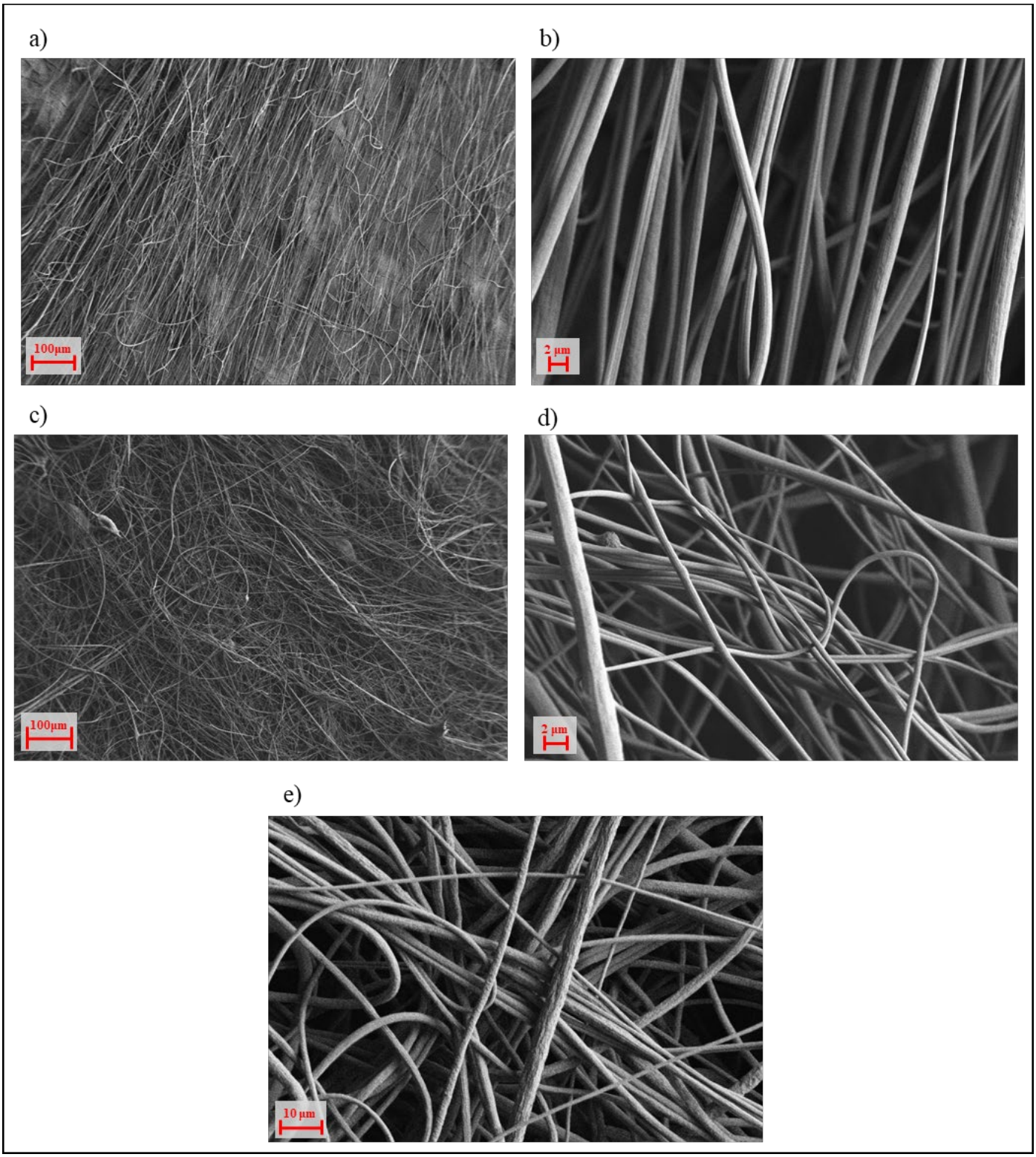

Figure 15: Fiber SEM micrographs at different scales. a) & b) PVDF control, c) & d) PVDF Ce-Sulfate 5%, and e) PVDF Ce-Nitrate 5% at 10 µm

Figure 15.c shows the micrograph for a PVDF Ce-Sulfate 5% sample. As seen, this time there is less fiber order regarding its alignment, and some beads can be perceived on the surface. Figure 15.d shows a section of PVDF Ce-Sulfate 5% fibers at higher magnification; fibers have a smooth surface morphology as well, with exception of a few beads. Figure 15.e shows the micrograph of the PVDF Ce-Nitrate 5%, and it can be noticed how the surface is different from that of the fibers with sulfate. The morphology for these samples appears to have a rougher texture, and the presence of a clear alignment is missing as well.

5.1.2 Fiber diameter analysis

From all the SEM images produced, the average fiber diameters were measured by statistical analysis and reported in Figure 16. Neat PVDF shows an average fiber diameter of 0.9 μm with a range of 0.8 to 1μm. The PVDF Cerium-Nitrates show higher average fiber diameter as compared to the PVDF Cerium-Sulfates. It is also noticeable that as the doping concentration increases, the fiber diameter increases; something that is present on both PVDF Cerium-Nitrates and PVDF Cerium-Sulfates.

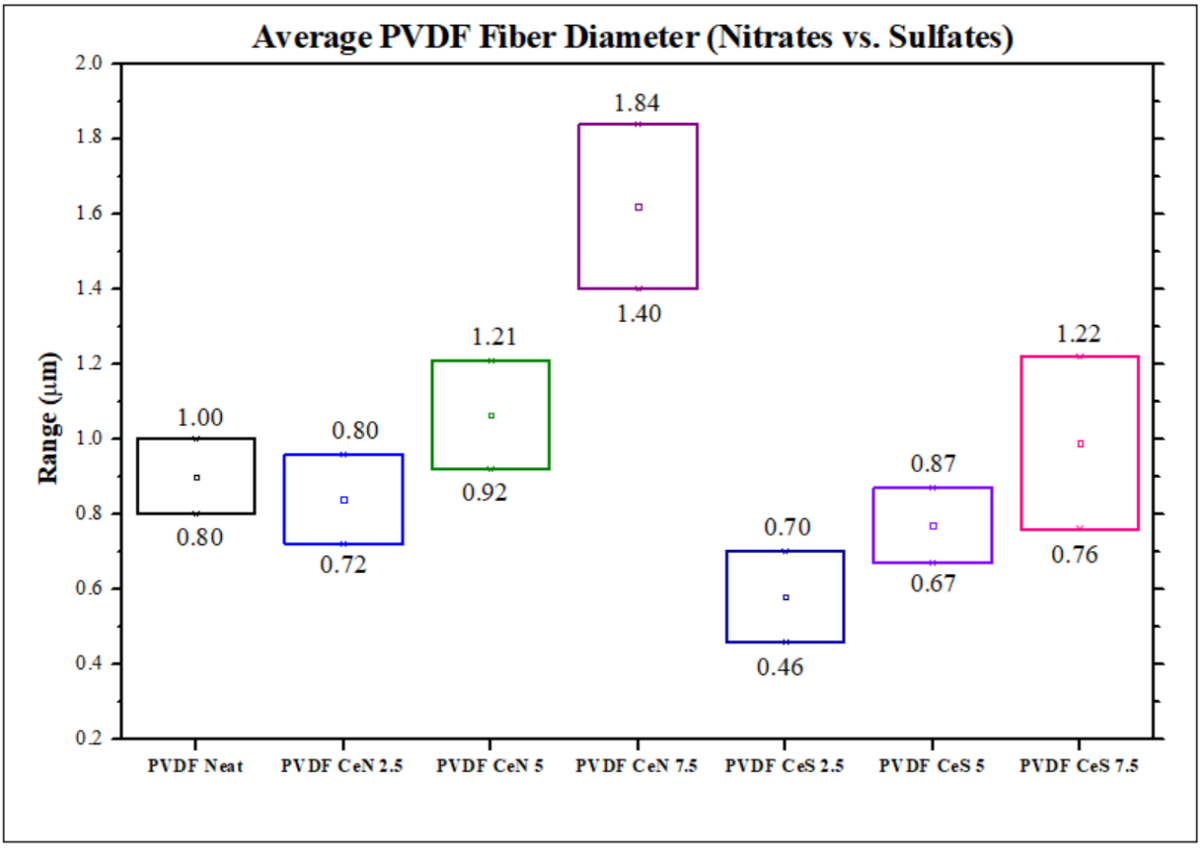

Figure 16: Average Fiber Diameter Range for PVDF Ce-Nitrates and PVDF Ce-Sulfates

The effect of fiber alignment played a role in fiber diameter as seen in Figure 17. For the fibers that were collected using the automatic rotating cylinder, as they were being spun, their diameters are smaller in comparison to the fibers manually collected. Only the PVDF Cerium-Sulfate fibers, as well as the PVDF fibers with graphene were used for comparison in this part due to their high production yield and their higher piezoelectric response; this will be explained in greater detail in section 5.3.

As seen in Figure 17, a similar trend as seen on Figure 20 occurs where the average diameter range increases with increasing doping concentration. The fiber diameter range for PVDF Ce-Sulfate 5% is 0.40-0.60 µm, and for 7.5% is 0.86-1.04 µm, which are smaller in comparison to the ranges for the same concentrations in the misaligned fibers. It can also be seen how the Graphene doped PVDF fibers had a decrease in average fiber diameter; there is a reduction in diameter by almost 50% from the original; 1.28-1.59 µm to 0.67-0.93 µm.

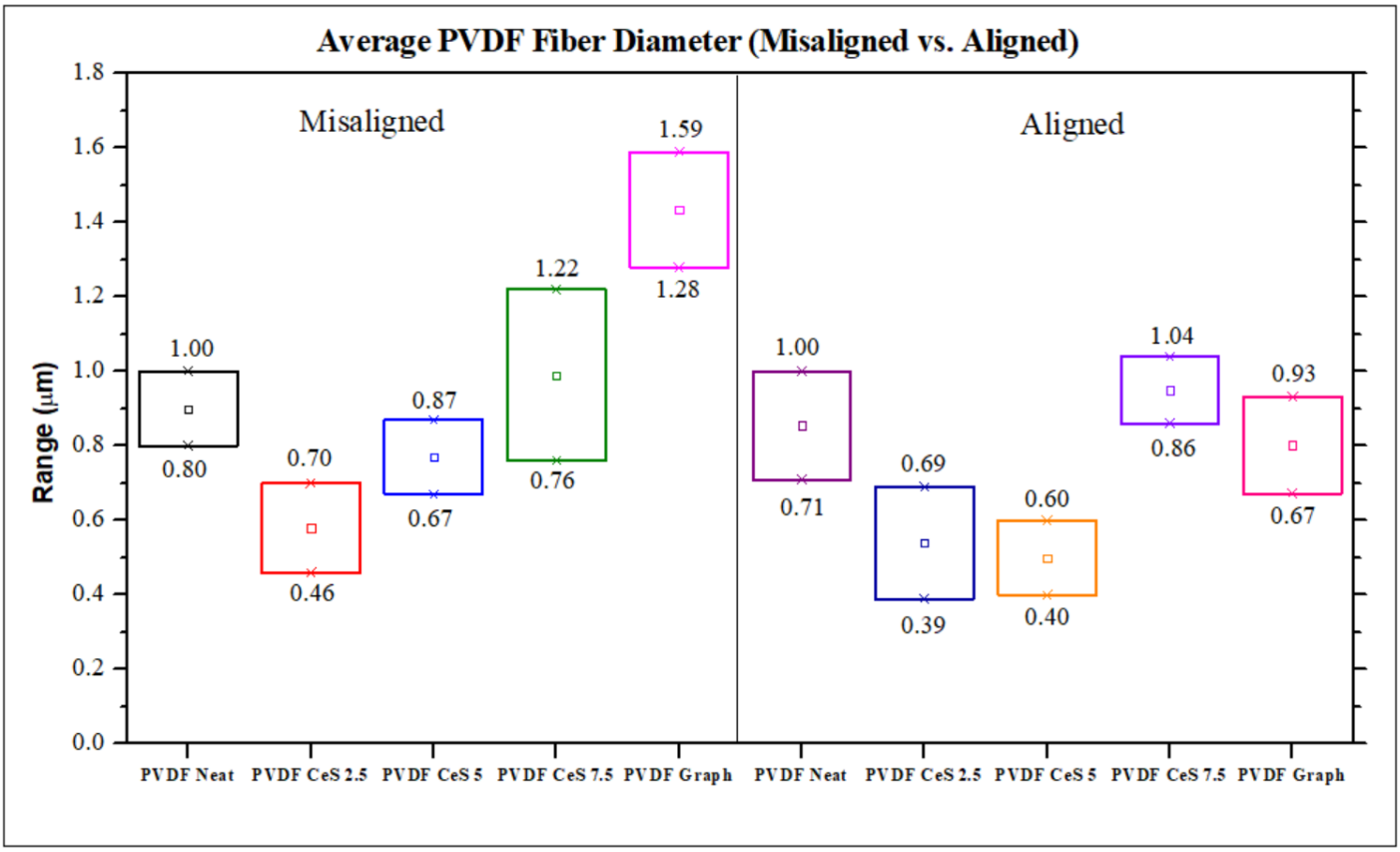

Figure 17: Average Fiber Diameter Range for aligned and misaligned PVDF fibers

5.2 FTIR Analysis

As mentioned in previous chapters, the piezoelectric effect of the PVDF strongly depends on the formation of the beta-phase. PVDF naturally exists on the alpha-phase, so mechanical or chemical work needs to be done to transform PVDF from a mostly alpha-phase to a mostly beta-phase. After processing, the samples were analyzed using FTIR to see the correlation between the doped and aligned on the beta-phase formation and the effect on diminishing the alpha-phase. Figure 18 shows the IR spectra for the PVDF control fibers, PVDF Cerium-Nitrates and Sulfates. At λ=1270 cm^{-1}, it can be observed that the peak increases for all samples when compared to the control sample, the PVDF in powder form. This peak corresponds to one of the beta-phase peaks in the PVDF.

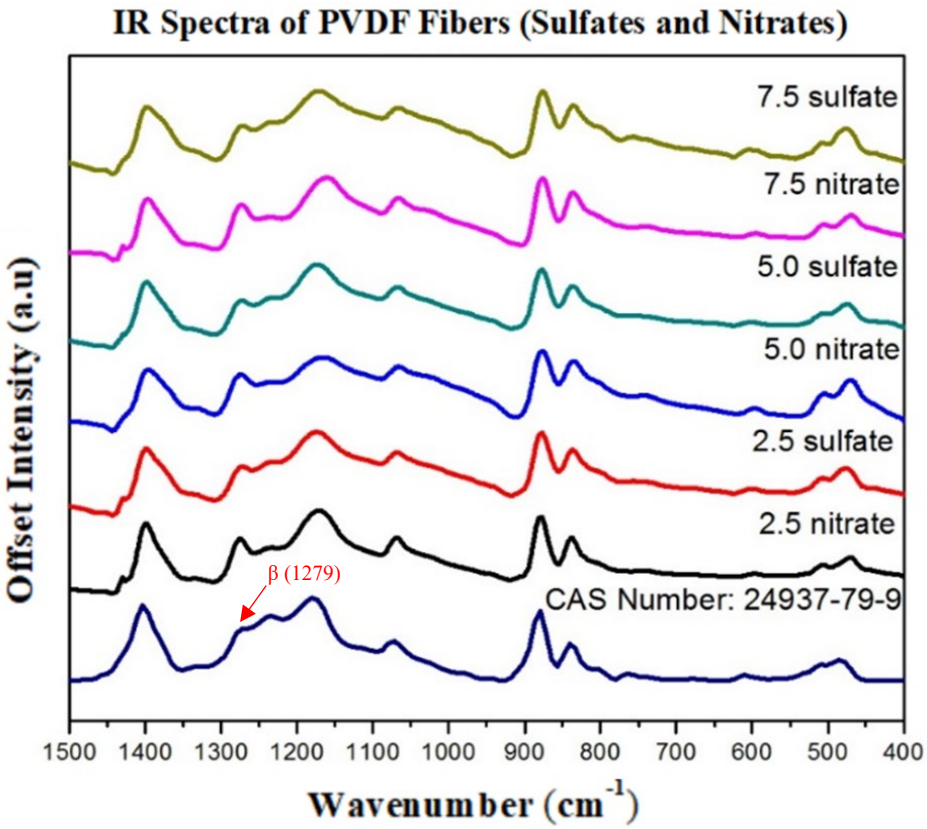

Figure 18: IR Spectra for PVDF Nitrate and Sulfate fibers

The beta-phase formation of the PVDF fibers was calculated using Beer-Lambert's Law (Equation 1). The values used for A_α and A_β correspond to the intensities of the sample being analyzed at 530 cm^{-1} and 840 cm^{-1} respectively. Table 7 shows a summary of the beta-phase formation for all the values tested. From this Table, it can be seen how fibers have a higher beta-phase formation in contrast to the powder; therefore, showing how mechanical alignment induces formation of the beta-phase. Another pattern that is clear is that for the most part, as the doping concentration increases, the beta-phase formation increases as well. The water molecules in the Cerium-complexes form hydrogen bonds with the hydrogen in the PVDF molecules which causes an increase in self-poling of the PVDF, thus a higher concentration of dopants, higher degree of poling.

Table 7: Beer-Lambert's Law for β-Phase Formation on PVDF Fibers

	Material	Intensity at Peak 530	Intensity at Peak 840	F(β)
Misaligned	PVDF Powder	0.08677	0.18547	**62.9%**
	PVDF Control	0.2340	0.5159	**63.6%**
	PVDF CeN 2.5	0.1601	0.4399	**68.6%**
	PVDF CeN 5	0.0809	0.2944	**74.3%**
	PVDF CeN 7.5	0.2246	0.6114	**68.4%**
	PVDF CeS 2.5	0.2050	0.5140	**66.6%**
	PVDF CeS 5	0.1543	0.3735	**65.8%**
	PVDF CeS 7.5	0.3130	1.0900	**73.4%**
	PVDF Graphene	0.02872	0.10232	**73.9%**
Aligned	PVDF Control	0.03527	0.09741	**68.7%**
	PVDF CeS 2.5	0.04797	0.15837	**72.4%**
	PVDF CeS 5	0.02575	0.09489	**74.5%**
	PVDF CeS 7.5	0.02594	0.09785	**75.0%**
	PVDF Graphene	0.05078	0.18606	**74.4%**
	PVDF-PPy-Graph	0.02889	0.102	**73.7%**

Also, from this Table the effect of fiber alignment on the beta-phase formation can be analyzed; the differences between aligned and misaligned fibers can also be observed in Figure 19. It can be seen how fiber alignment increases the formation of the beta-phase; the values are higher than the misaligned fibers. It is worth noticing that the addition of graphene to the PVDF does induce beta-phase formation, although there is a small change between the aligned and misaligned PVDF fibers with graphene; however this small change does have a pronounced effect as it will be seen further in the chapter when analyzing the voltages.

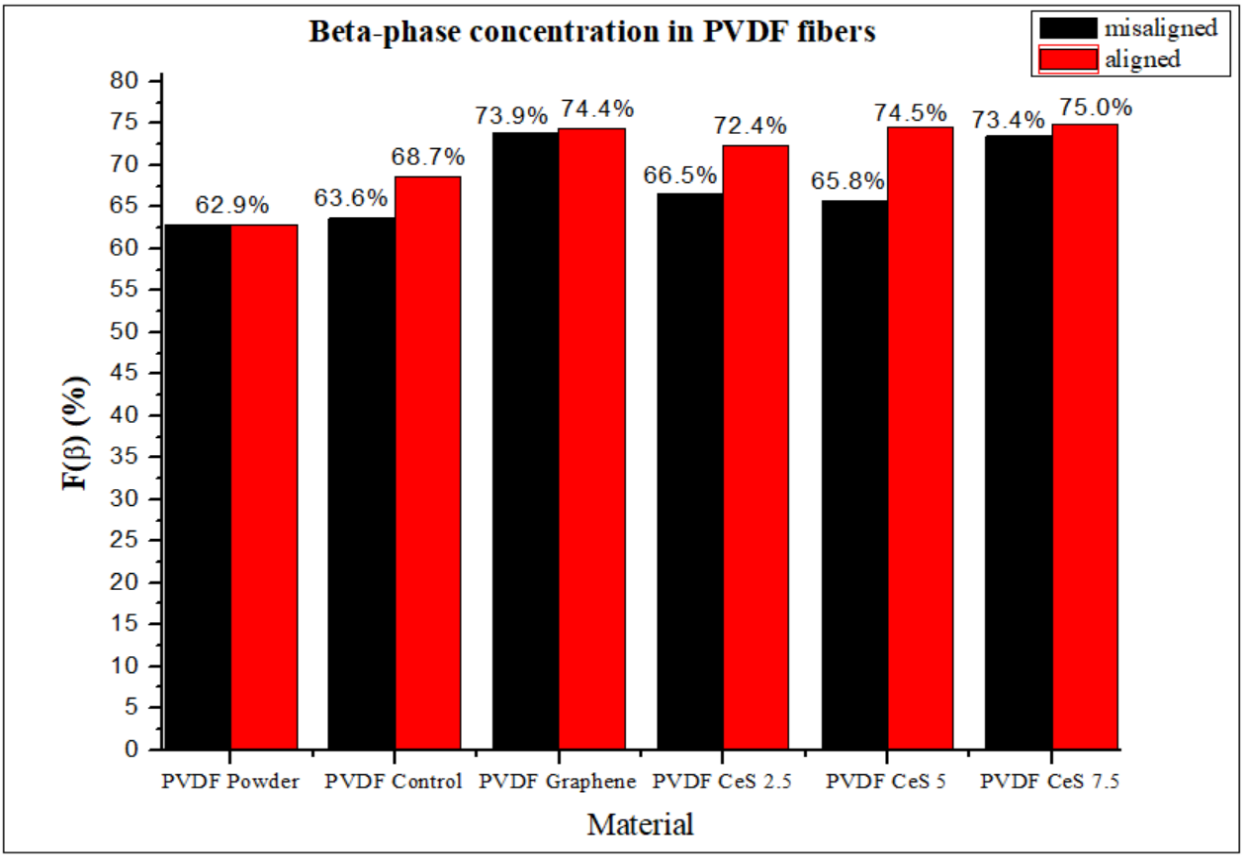

Figure 19: Comparison between aligned and misaligned PVDF fibers

Figure 20 and Figure 21 both show the FTIR spectra for the aligned PVDF Ce-Sulfate fibers, one from 1500-400 cm^{-1}, while Figure 21 shows just the section between 1000-400 cm^{-1}.

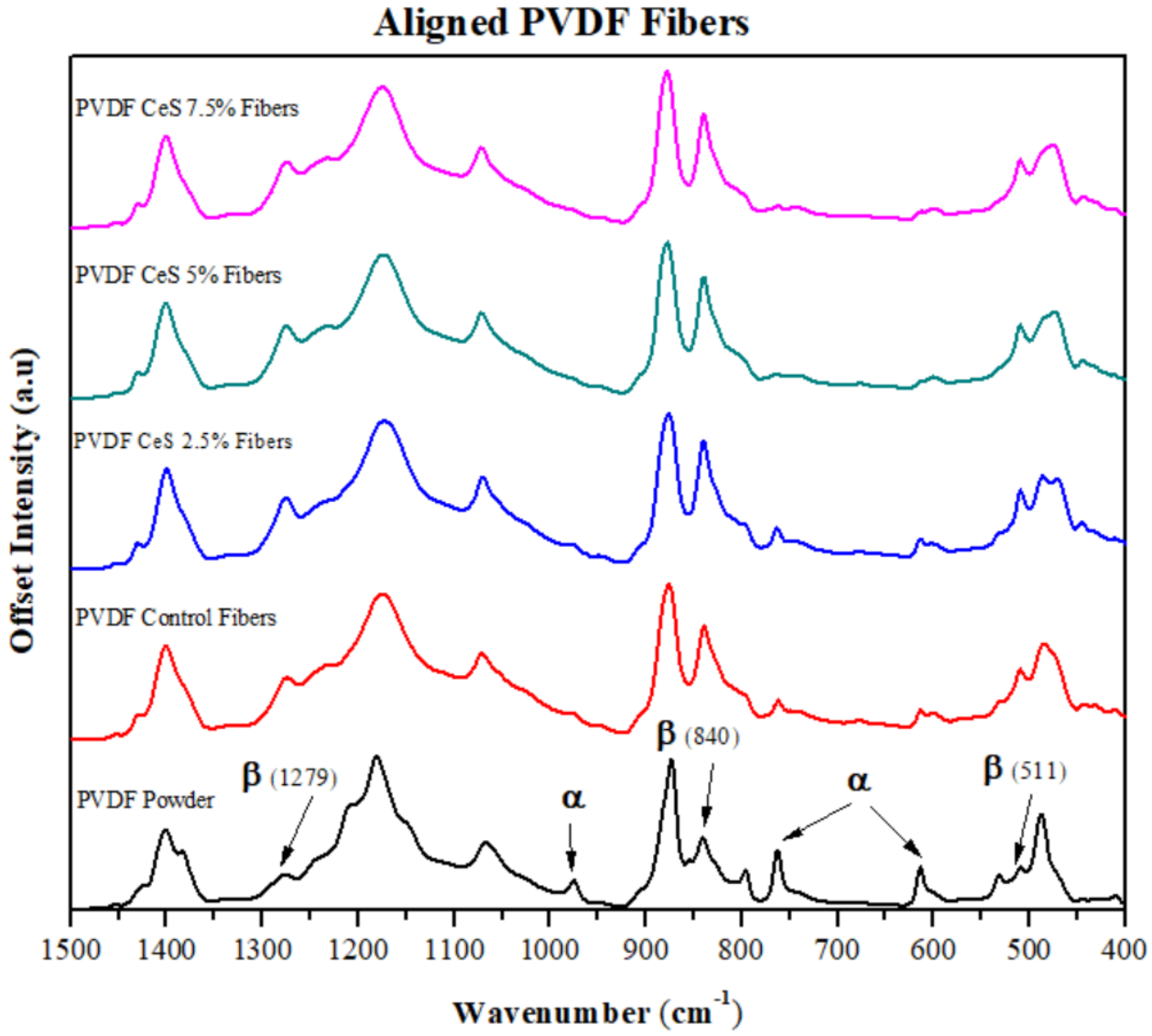

Figure 20: IR spectra for aligned PVDF fibers

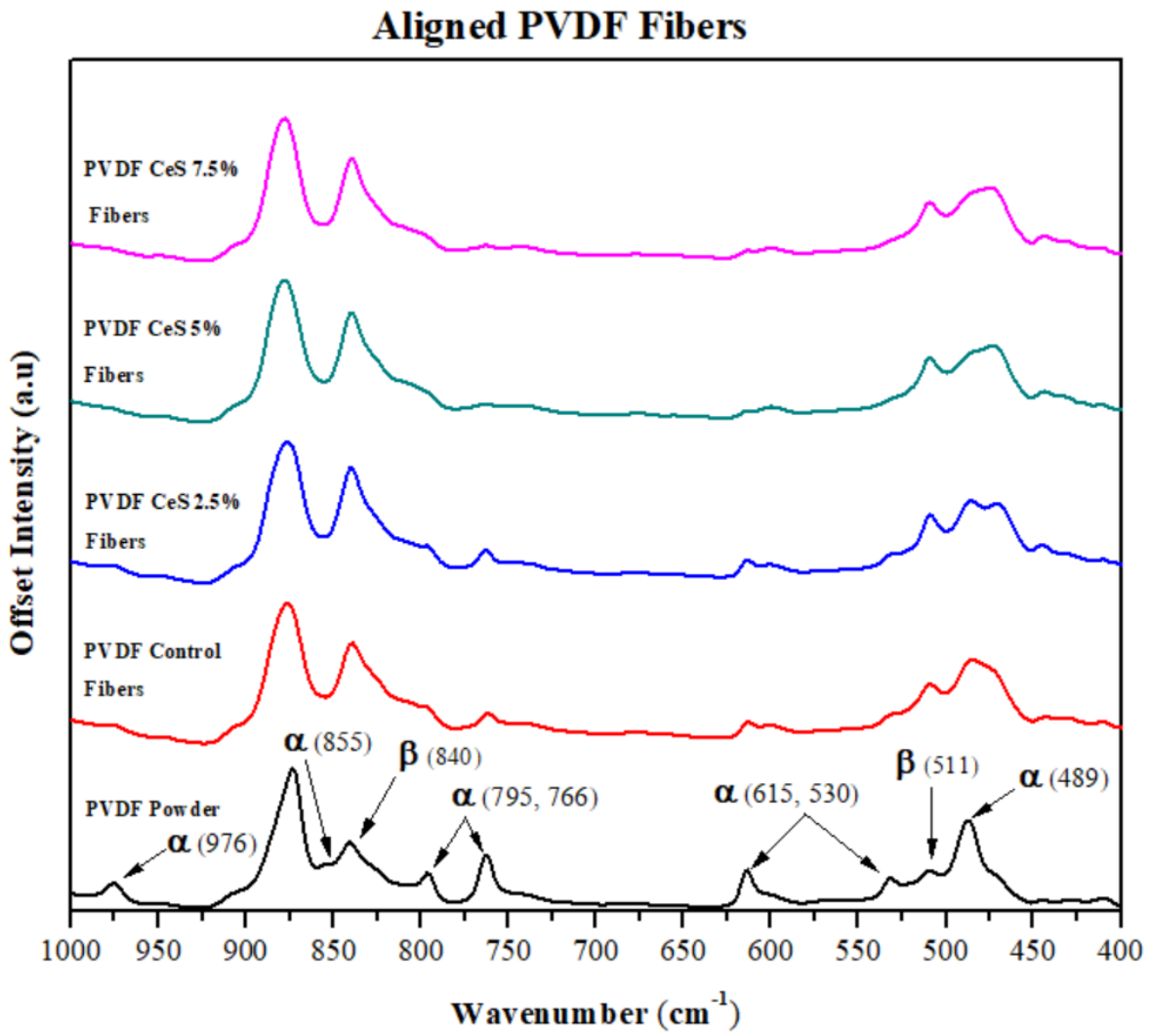

Figure 21: IR spectra for aligned PVDF fibers between 1000 to 400 cm^{-1}

5.3 Voltage Analysis

Piezoelectric properties were evaluated on all developed mats. The plots produced by the neat or control PVDF fibers (fibers without dopants), during finger tapping showed a peak-to-peak voltage of 1.52V, where the maximum positive voltage was 1.0V and the minimum -520mV. This signal shape as seen on Figure 22 is common on all piezoelectric responses; there is an impulse (a peak), a decrease (a valley), and a small ramped response plus some overshoot before returning to the original state.

5.3.1 PVDF Ce-Nitrates vs PVDF Ce-Sulfates

The data shown in Figure 22 show the voltage response for the Ce-doped PVDF fibers when struck using the PVDR-Pro Tester. In contrast to the repeatedly finger tapping, this controlled test uses a pneumatic cylinder striking the fibers constantly at 35 psi for 10 min, with a frequency of 1.16 Hz. A similar trend to the neat PVDF fibers appears, except the response is much higher, 2.24 V of maximum voltage and a peak-to-peak voltage of 4.12 V. The response seems to decrease as fast as it increases, with a period of 5ms for the complete response. From Figure 23, a consistent and repetitive piezoelectric response can be observed from the PVDF fibers created with different percentages of sulfates or nitrates. Figure 23 illustrates the voltages produced using the pneumatic apparatus to apply controlled pressure. As it can be seen, the piezoelectric response, or peak-to-peak voltage response, seems to follow a trend increasing after each subsequent round. The highest peak-to-peak voltage recorded was above 8.5 V for the for the PVDF Ce-Sulfate 5% fibers. It is observed that neat PVDF fibers show higher response than systems doped with cerium nitrate.

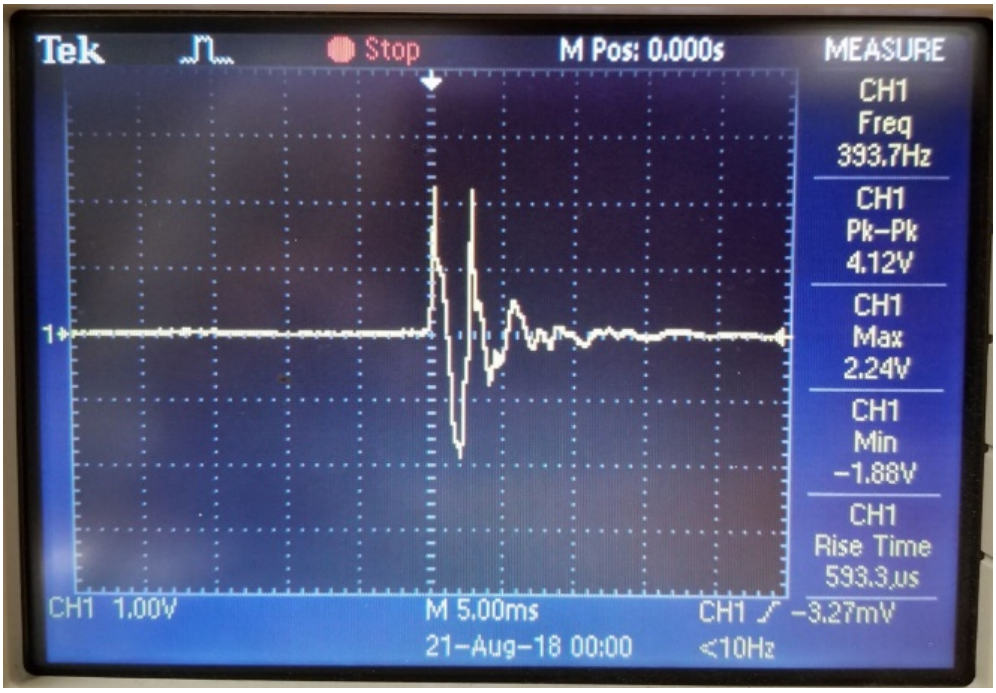

Figure 22: Oscilloscope view of voltage peaks produced by PVDF-Ce fibers with PVDR-Pro

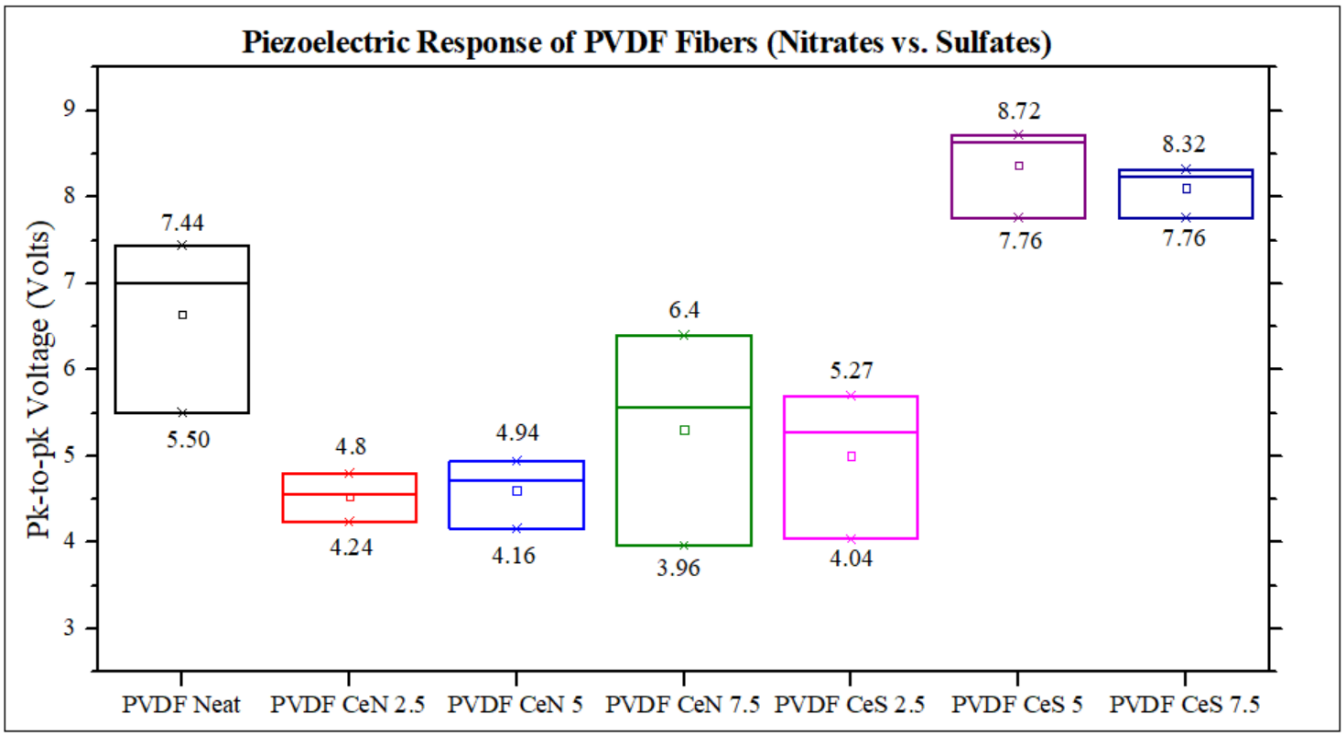

Figure 23: Voltages produced using PVDR PRO for all Nitrate and Cerium fibers

5.3.2 PVDF fibers: aligned vs misaligned

Figure 24 shows the comparison in voltages for aligned and misaligned samples. Voltage testing with aligned fibers shows higher voltage response. Aligned PVDF Neat sample produced a peak-to-peak voltage range between 8-10 Volts. A similar trend is found in aligned fibers as in the misaligned samples. In both tests, PVDF Ce-Sulfate 5% yields the highest voltage under control conditions; 7.76-8.64 V for the misaligned, and 9.20-11 V for the aligned fibers. As it can be seen, the fibers that showed greater piezoelectric response had a higher beta-phase formation; a clear indication of the relationship between the increase poling of the fibers by mechanical alignment and the piezoelectric response.

According to Figure 24, doping of PVDF with graphene particles yields a higher piezoelectric output than Ce-Nitrate or Ce-Sulfate as seen on the graph; 9.5-11.5 V, and 11-12.2V, for the misaligned and aligned fibers respectively. This is related to the results from Figure 23, where PVDF-Graphene have one of the highest beta-phase formations. There is a smaller difference between the voltages of the aligned and misaligned PVDF-Graphene, which corresponds to the small difference in beta-phase formation for both samples.

PVDF samples were doped with graphene to determine whether the conductivity of the fibers would increase, since graphene is known for being a good conductor. Figure 25 shows the voltage response for a rapid finger tapping on a PVDF-Graphene sample. As seen, the response is continuous; while other samples may or may not respond the same to every impact, PVDG-Graphene shows increase sensitivity to both high and low-magnitude impacts. Figure 26 shows the voltage response for the aligned PVDF-Graphene; it can be noticed how the signal is composed of one peak only instead of many as seen in Figure 22.

This signal pattern was found in most PVDF-Graphene fibers during piezoelectric testing; the exact nature of this effect is unknown, but it will be subjected to further testing to understand the principles behind.

As on Chapter 2, the piezoelectric effect is pressure dependent, meaning that an increase in force applied should produce a proportional increase in the voltage output, all other parameters constant; this relationship can be seen in Figure 27, where the voltage throughout of aligned PVDF-Graphene fibers increased with increasing applied pressure. The maximum voltage response obtained was between 18.8 to 26.4 V with a pressure of 55 psi.

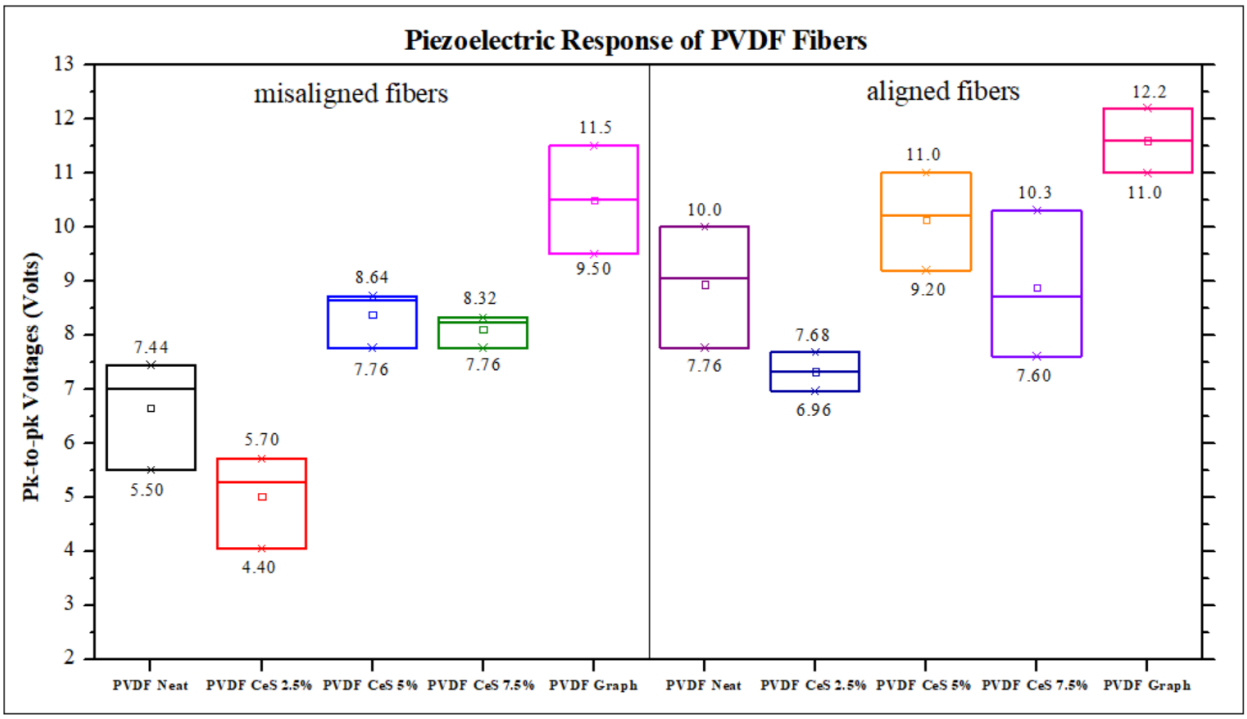

Figure 24: Voltages produced using PVDR PRO for aligned and misaligned PVDF fibers

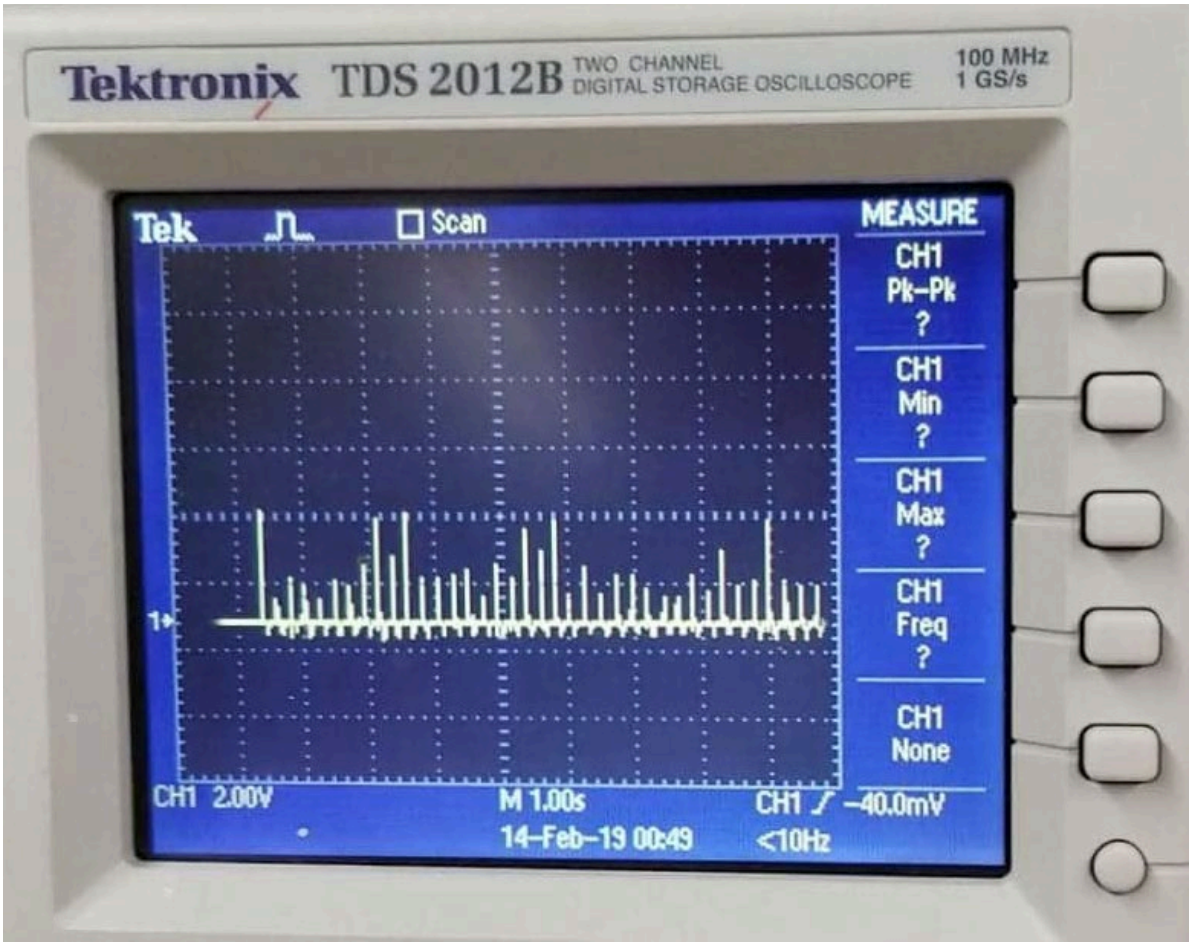

Figure 25: Voltages produced by finger tapping for aligned PVDG-Graphene fibers

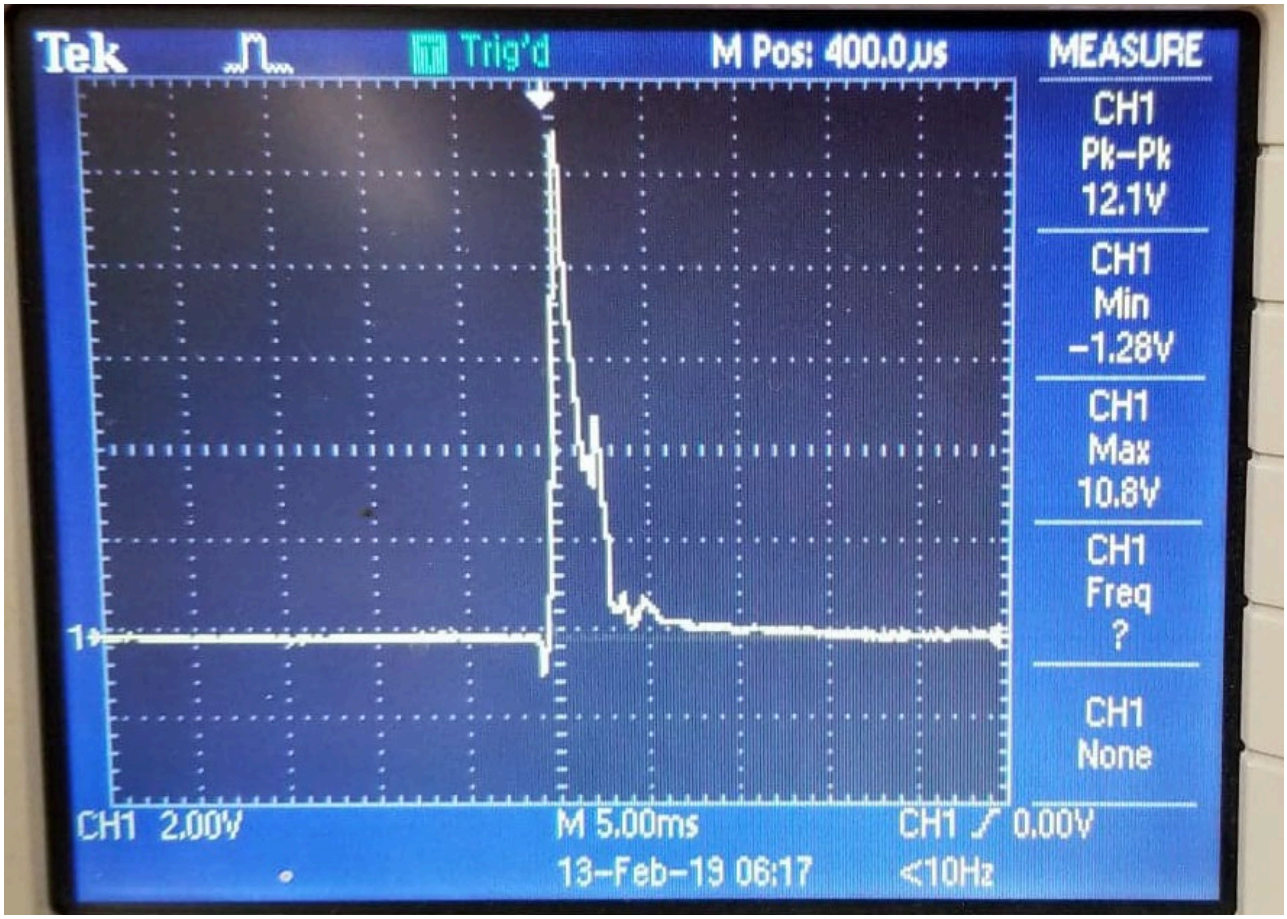

Figure 26: Voltage signal by PVDR-Pro for aligned PVDG-Graphene fibers

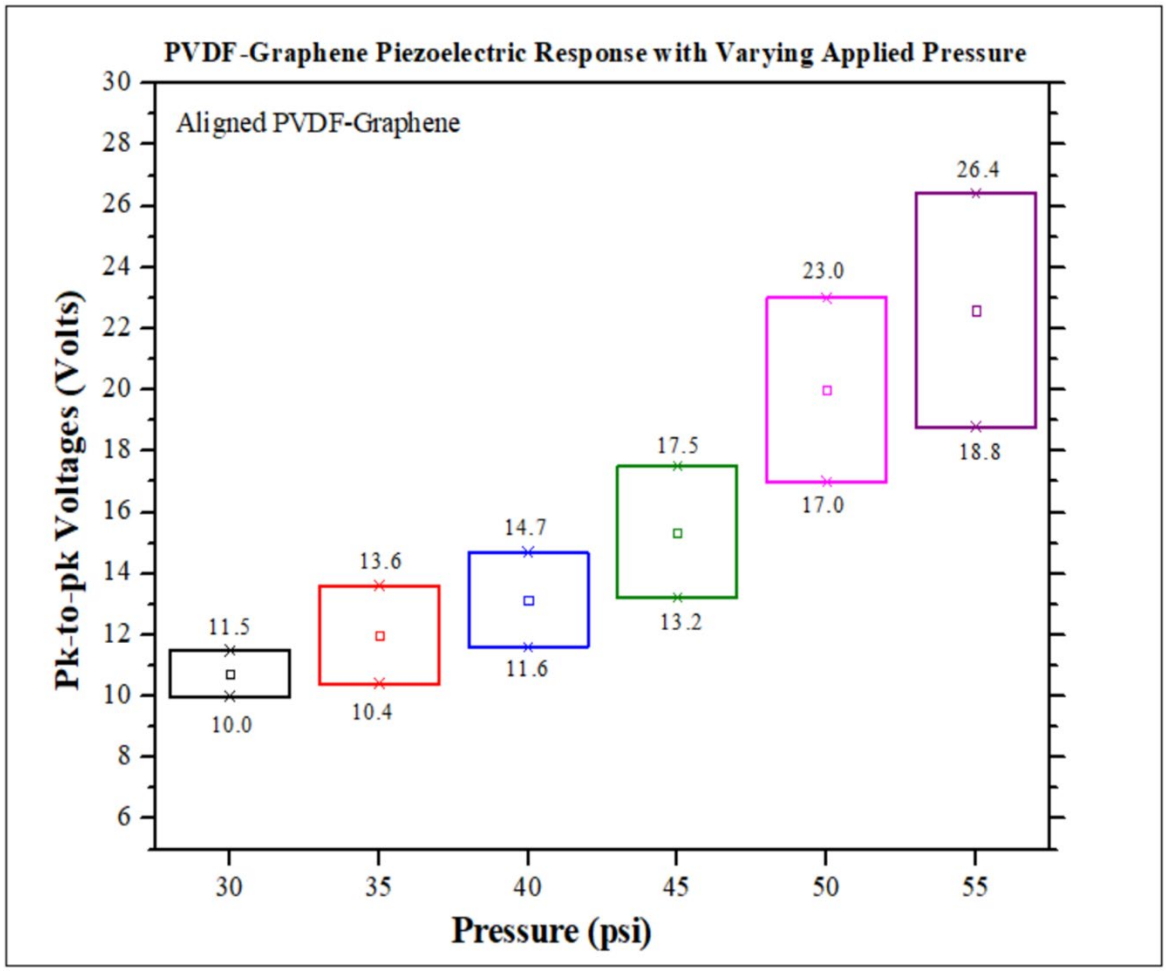

Figure 27: Piezoelectric response for aligned PVDG-Graphene fibers with increasing pressure

5.4 Polypyrrole Coating and Doping

Fibers were coated with Polypyrrole to determine if their conductivity would increase and affect the voltage response. Different coating methods were used to successfully coat fibers. The summary of the results for each coating are listed in Table 8.

Table 8: Polypyrrole coating summary

Method	Type	Materials used	Result
1	Pure PPy coating	5 wt.% PPy dispersion in water	Hydrophobicity of the fiber prevents coating
2	PPy dilution in water	5 wt.% PPy dispersion in water, water	Hydrophobicity of the fiber prevents coating
3	Iron Nitrate-Water-PPy with DMA and Acetone	5wt.% PPy dispersion in water, Iron (III) Nitrate-nonahydrate, water	Hard to wet; better PPy absorption after wetting
4	Iron Nitrate Solution with Solvents	5wt.% PPy dispersion in water, Iron (III) Nitrate-nonahydrate, water, DMA, Acetone	Faster absorption; with high solvent concentrations fibers dissolve
5	Ppy-ethanol dilution in water	5 wt.% PPy dispersion in water, ethanol, water	Not enough PPy absorbed
6	Ppy dilution with ethanol coating	5 wt.% PPy dispersion in water, ethanol, water	Fibers lightly coated with PPy solution
7	Pure PPy with ethanol coating	5 wt.% PPy dispersion in water, ethanol	Faster absorption; fiber fully coated; fiber becomes fragile
8	High conductivity PPy with ethanol coating	Polypyrrole composite with carbon black, ethanol	Fibers lightly coated with PPy; coating easy to take off by touch; does not stay coated

Polypyrrole coating proved to be disadvantageous regarding its results. Although some methods proved adequate for coating the PVDF fibers, they yielded little to no voltage when testing; the highest of values being lower than 3 Volts, less than Neat PVDF. Unfortunately, coating decreased the mechanical properties of the fibers; flexibility and strength of the fibers were decreased; fibers were easier to tear and did not stretch as much, thus reducing the output voltage. When tested for conductivity, the fibers were not able to be used as conductor; the fibers did not let current pass as to bridge the gap between anode and cathode to light up an LED.

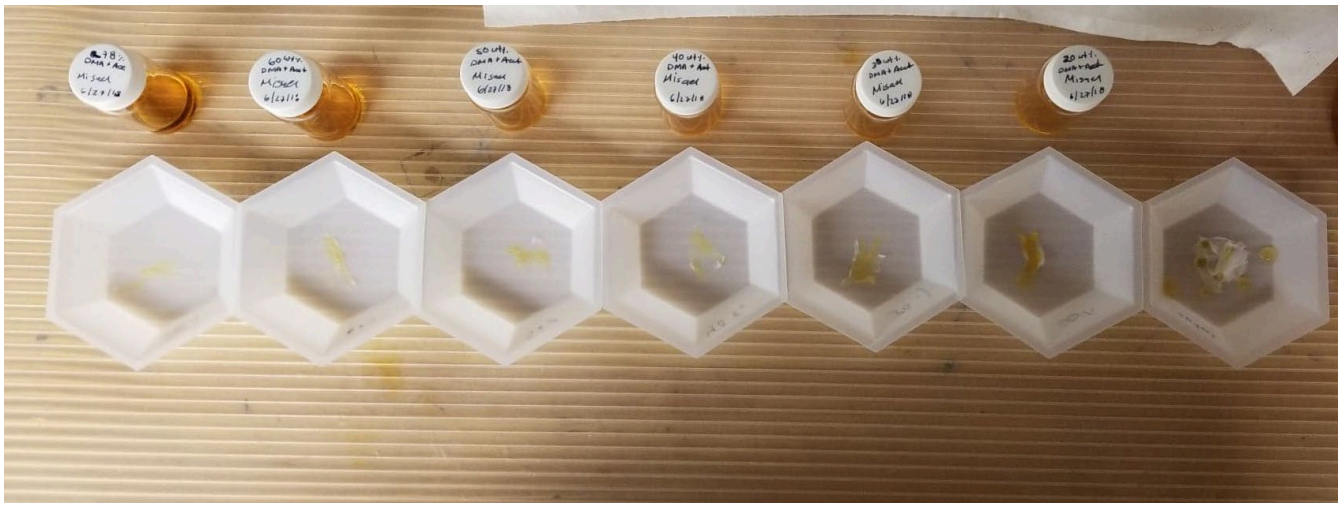

Figure 28: Coating method 4. Fiber samples with different concentrations of solvents

Figure 29: Coating method 7. Fiber samples after coating

In contrast to the PPy coating, doping the fibers with PPy produces better results. Despite fiber production being difficult whenever fibers are produced and tested for piezoelectricity, they can produce higher voltages in contrast to the coating methods. These fibers yielded a peak-to-peak voltage of 3.72 Volts; much less than the fibers already presented. PVDF fibers doped with a conjugated polymer of Polypyrrole resulted in faster charge/discharge rates with smoother voltage signal. The fibers were able to auspiciously charge a 10μF capacitor, however more testing needs to be done regarding a more efficient energy harvesting circuit. Nevertheless, the complexity and difficulty of PVDF-PPy fiber production is due to the highly-conductive PPy powder not dissolving correctly in the solution and getting stuck on the spinnerete, preventing fiber formation during Forcespinning®; as such, this method requires more in-depth analysis and research to improve the results and make it a viable alternative in comparison to graphene doping.

Figure 30: PVDF-PPy doped fiber sample

5.5 Thermal Analysis

Thermophysical analysis of the developed systems was conducted using differential scanning calorimetry (DSC) and thermogravimetric analysis (TGA). As it was observed in the FTIR analysis, the polymer experienced molecular alignment. Figure 31.a shows the endothermic DSC analysis; this graph shows apparent negligible changes in the melting peak, however when analyzing the melting enthalpy of each sample a pattern emerges. To calculate the enthalpy, the area under the DSC melting curve was taken for each sample from 150-180 °C. As seen, the Neat PVDF fibers have a higher melting enthalpy than the raw PVDF powder, and consequently a higher crystallinity as depicted in Figure 31.c. It is also observed that the samples with 5 wt.% of Cerium, both Nitrate and Sulfate, have the highest melting enthalpy and crystallinity, followed by the samples with 2.5 wt.% concentration, and then with 7.5 wt.% concentration for Nitrates, and the opposite for Sulfates (7.5 wt.% then 2.5 wt.%).

The exothermic graphs are presented in Figure 31.b; in here it can be observed that the presence of the Cerium produces a nucleating effect. This nucleation effect increases as the Cerium concentration increases. This change is independent of processing given that the cooling analysis occurs after the processing history is deleted by subjecting the samples to isothermal heating at 250 °C for 10 minutes. As seen as in Figure 31.d, the crystallinity of the samples increases with increasing doping concentration, where both samples with 5wt. % dopant concentration show the highest crystallinity. By round 2, the thermal history is erased, and the crystallinity decreases, however the same trend as in round 1 continues. It is worth noticing that the numbers for melting enthalpy are very similar to the crystallinities as seen from Figures 31.c & 31.d; this might be in part due to the fact that the melting enthalpy is related to the crystallinity of the sample, and thus they are very similar.

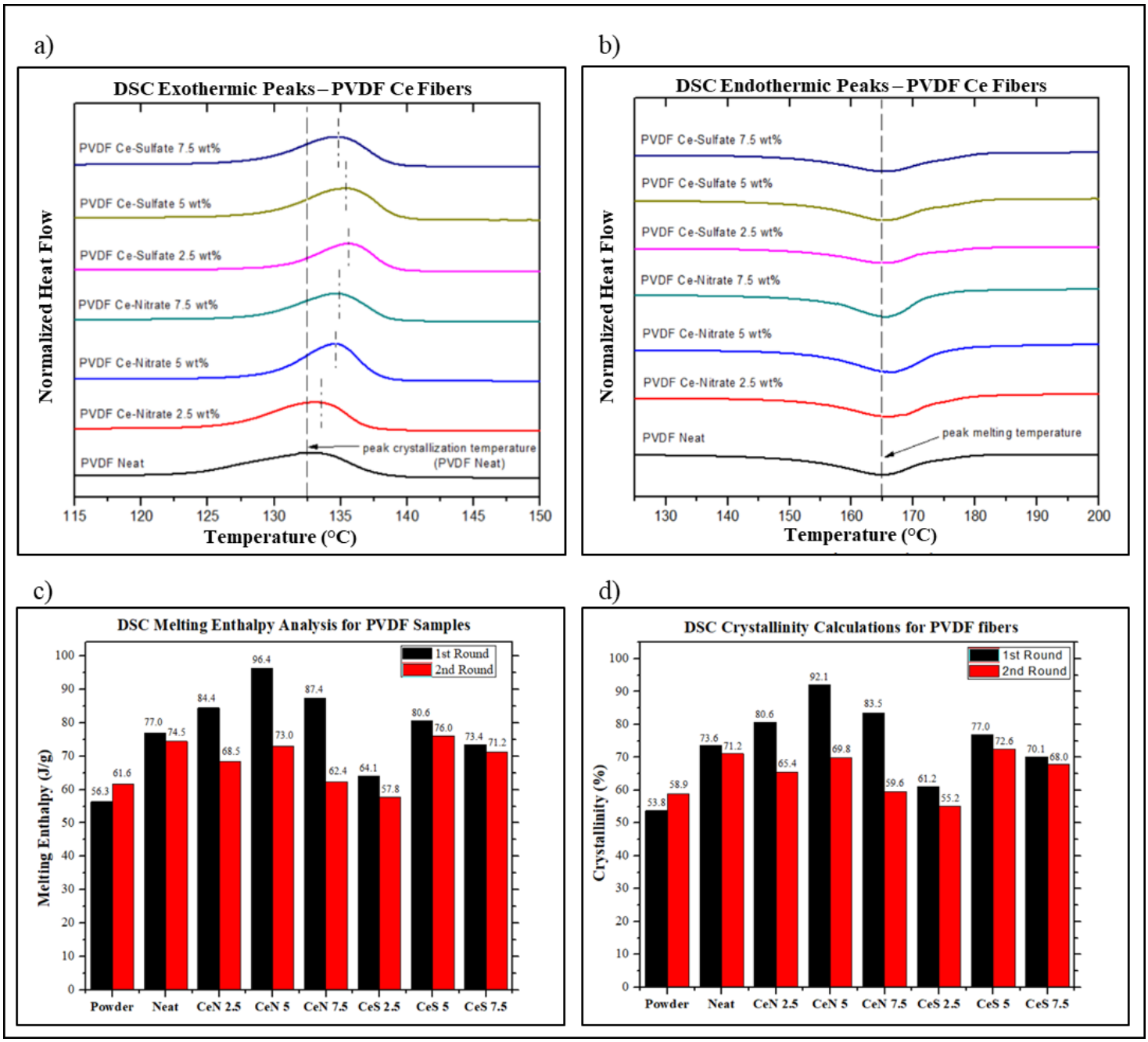

Figure 31: DSC Analysis for PVDF fibers. 1st Round a) Exothermic and b) Endothermic peaks, c) calculated melting enthalpies, and d) calculated crystallinities

Figure 32 shows the TGA results for the developed membranes. It can be observed that the pure PVDF samples show a higher degree of water absorption as depicted by the 2.4 wt.% drop observed at 100 °C. Another distinctive drop is observed at 200 °C for the Cerium nitrate samples which is observed to increase upon increasing cerium nitrate content. The ultimate degradation temperature for the fibers varied from 430 °C for the Bulk PVDF, to 447 °C for the cerium doped fibers. Although cerium nitrate and cerium sulfate degraded 100% on their raw state, when used as dopants on the PVDF nanofibers it is observed that there is a synergy among the PVDF and the cerium complexes. The order of degradation from least to most is as follows: Neat PVDF fibers at 25 wt.% remaining, PVDF Cerium Sulfate fibers at 22 wt.% with an exception of PVDF CeS 7.5, and PVDF Cerium Nitrate fibers at 18 wt.% according to Figure 32.

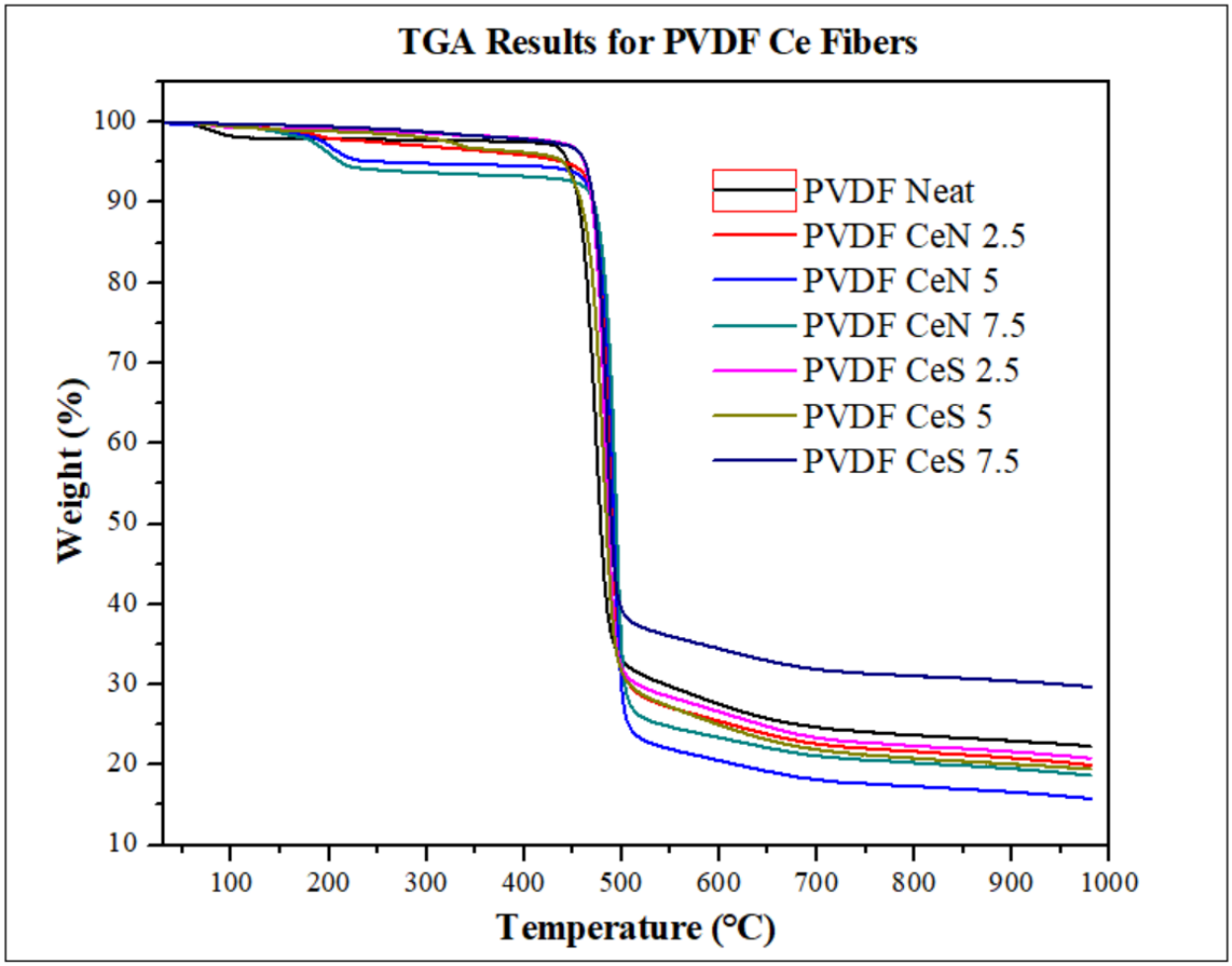

Figure 32: TGA results for PVDF fibers

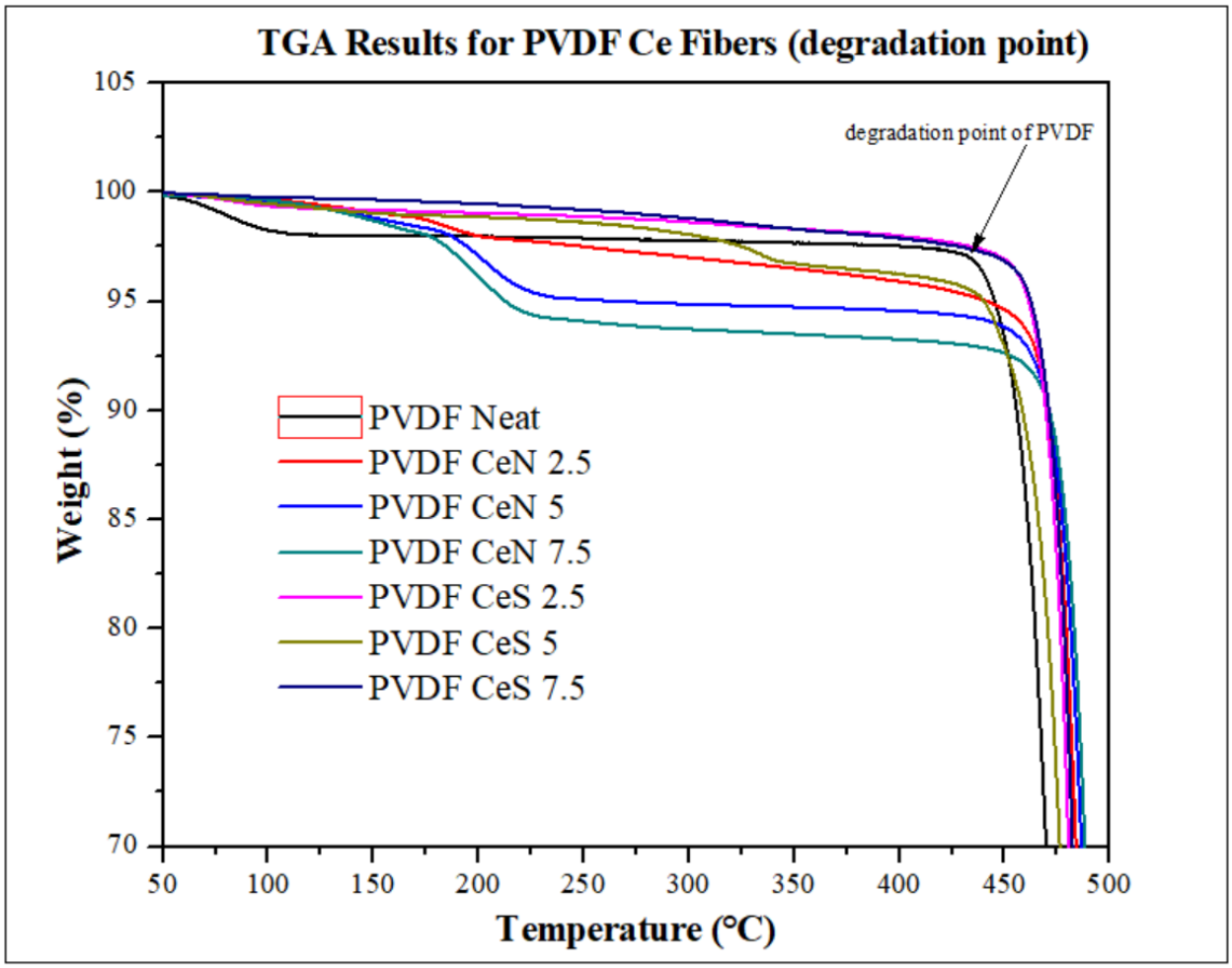

Figure 33: TGA results for PVDF fibers zoomed in at degradation point

CHAPTER VI

CONCLUSION

The scope of this study was to enhance the piezoelectric response of the PVDF Forcespun fibers by controlling the self-poling mechanisms—doping of Cerium-complexes and fiber alignment—in order to create light, flexible, and cost-efficient nanogenerators that can be used as an alternative method for energy harvesting applications. After careful testing and data analysis, the following conclusions can be made regarding this project.

The β-phase conformation of the PVDF fibers was achieved through the formation of 1D structures that prompted molecular alignment. The fiber mats were developed using the Forcespinning® technique.

Fibers were collected both with a minor degree of alignment and no further extensional elongation, and with a controlled directional alignment providing elongation. Cerium complexes were added to the PVDF solutions to evaluate its contribution to the self-poling mechanism, to overcome the lack of high degree of alignment and therefore ability to pole the system through post processes. FITR studies showed that the alpha-phase decreases with increasing dopant, while the beta-phase formation increases.

The cerium complexes provided an increase in the piezoelectric properties. The highest observed peak-to-peak voltages in the neat PVDF fiber mats was 7V while that one for the doped (cerium sulfate) PVDF fibers was 8V for misaligned fibers. It was observed that the addition of

cerium nitrate shows a piezoelectric response lower than the neat PVDF mats. Fiber alignment proved beneficial for the piezoelectric response; the average fiber diameter range decreased for most fibers, while increasing the beta-phase formation in comparison to the misaligned fibers. Thus, higher voltage responses were obtained with the highest value being between 9-11V.

The addition of graphene increased the sensitivity of the PVDF fibers and produced a higher voltage up to 12.2 V due to an increase in the beta-phase formation. The scope of these study was met; the piezoelectric response of the PVDF fibers was in fact enhanced by the methods described in this work; further research will be done regarding the combination of PVDF, Cerium-Sulfates, and Graphene into one set of fibers for further piezoelectric enhancement.

Further work required will be to efficiently test the fibers for energy harvesting by connecting them to a bridge rectifier circuit; also, an in-depth study will follow regarding the efficiency of the energy harvesting circuit, and its usefulness for practical applications.

REFERENCES

[1] Achaby, M. E., Arrakhiz, F. Z., Vaudreil, S., Essassi, E. M., & Qaiss, A. (2012). Piezoelectric β-polymorph formation and properties enhancement in graphene oxide – PVDF nanocomposites films. *Applied Surface Science,* 258, 7668-7677.

[2] Abolhasani, M. M., Shirvanimoghaddam, K., & Naebe, M. (2017). PVDF/Graphene composite nanofibers, with enhanced piezoelectric performance for development of robust nanogenerators. *Composites Science and Technology,* 138, 49-56.

[3] Andre, J. M., & Ladik, J., (1975). Electronic Structures of Polymers and Molecular Crystals. *Plenum Press,*

[4] Andrew, J. S., & Clarke, D. R., (2008). Effects of Electrospinning on the Ferroelectric Phase Content of Polyvinylidene Difluoride Fibers. *Langmuir*, 24, 670-672

[5] Aphale, A., Maisuria, K., Mahapatra, M. K., Santiago, A., Singh, P., & Patra, P. (2015). Hybrid Electrdoes by In-Situ Integration of Graphene and Carbon-Nanotubes in Polypyrrole for Supercapacitors. *Scientific Reports,* 5(14445), 1-8.

[6] Becker, R. O., & Marino, A. A. (1982). Chapter 4: Electrical Properties of Biological Tissue (Piezoelectricity). *Electromagnetism & Life. Albany, New York: State University of New York Press.* ISBN 0-87395-560-9.

[7] Birkholz, M. (1995). Crystal-field induced dipoles in heteropolar crystals – II: Physical significance. *Physik B - Condensed Matter*, 96(3), 333–340.

[8] Bormashenko, Y., Pogreb, R., Stanvsky, O., & Bormashenko, E. (2004). Vibrational spectrum of PVDF and its interpretation. *Polymer Testing,* 23, 791-796.

[9] Chang, C., Fuh, Y. K., & Lin, L. (2009). A direct-write piezoelectric PVDF nanogenerator. *15th International Conference on Solid-State Sensors, Actuators and Microsystems, Denver*, 1485-1488.

[10] Chang, J, Dommer, M., Chang, C., & Lin, L. (2012). Piezoelectric nanofibers for energy scavenging applications. *Nano Energy*, 1(3), 356–371.

[11] Chang, W.Y., & Hsu, C. H. (2018). Electromechanical Characteristics of Polyvinylidene fluoride for Flexible Electronics. *Transactions of the Canadian Society of Mechanical Engineering,* 37(3), 325-333.

[12] Chanunpanich, N., Byun, H., & Kang, I. (2006). Membrane morphology: phase inversion to electrospinning. *Membrane Journal*, 16, 133.

[13] Chee, W. K., Lim, H. N., & Huang, N. M. (2014). Electrochemical properties of free-standing Polypyrrole/graphene oxide/zinc oxide flexible supercapacitor. *International Journal of Energy Research,* 39, 111-119.

[14] Chen, H., Han, S., Liu, C., Luo, Z., Shieh, H. D., Hsiao. R., Yang, B. (2016). Investigation of PVDF-TrFE composite with nanofillers for sensitivity improvement. *Sensors and Actuators A: Physical.* 245, 135-139.

[15] Chen, X., Xu, S. Y., Yao, N., & Shi, Y. (2010). 1.6 V Nanogenerator for Mechanical Energy Harvesting Using PZT Nanofibers. *Nano Letters*, 10, 2133-2137.

[16] Chougule, M. A., Pawar, S. G., Godse, P. R., Mulik, R. N., Sen, S., & Patil, V. B. (2011). Synthesis and Characterization of Polypyrrole (PPy) Thin Films. *Soft Nanoscience Letters,* 1, 6-10.

[17] Dahiya, R. S., Cattin, D., Adami, A., Collini, C., Barboni, L., & Valle, M. (2011). Towards Tactile Sensing System on Chip for Robotic Applications. *IEEE Sensors Journal*, 11(12), 3216–3226.

[18] Dillon, D. R., Tenneti, K. K., Li, C. Y., Ko, F. K., Sics, I., & B. S. Hsiao. (2006). On the structure and morphology of polyvinylidene fluoride-nanoclay nanocomposites. *Polymer,* 47, 1678-1688.

[19] Dong, W., Xiao, L., Hu, W., Zhu, C., Huang, Y. A., & Yin, Z. (2017). Wearable human-machine interface based on PVDF piezoelectric sensor. *Transactions of the Institute of Measurements and Control,* 39(4), 398-403.

[20] Doshi, J., & Reneker, D. (1995). Electrospinning process and applications of electrospun nanofibers. *Journal of Electrostatics*, 35(2), 151-160.

[21] Fang, J., Wang, X., & Lin, T. (2011). Electrical power generator from randomly oriented electrospun poly(vinylidene fluoride) nanofibre membranes. *Journal of Materials Chemistry,* 21, 11088-11091.

[22] Fridleifsson, I. B. (2001). Geothermal energy for the benefit of the people. *Renewable and Sustainable Energy Reviews*, 5(3), 299-312.

[23] FTIR Basics. ThermoFisher Scientific. Image obtained from https://www.thermofisher.com/us/en/home/industrial/spectroscopy-elemental-isotope-analysis/

[24] Furukawa, T. (1989). Ferroelectric properties of vinylidene fluoride copolymers. *Phase Transitions*, 18(3), 143–211.

[25] Gaihre, B., Alici, G., Spinks, G. M., & Cairney J. M. (2010). Synthesis and performance evaluation of thin film PPy-PVDF multilayer electroactive actuators. *Sensors and Actuators A: Physical,* 165, 321-328.

[26] Garain, S., Jana, S., Sinha, T. K., Mandal, D. (2016). Design of In Situ Poled Ce^{3+}-Doped Electrospun PVDF/Graphene Composite Nanofibers for Fabrication of Nanopressure Sensor and Ultrasensitive Acoustic Nanogenerator. *Applied Materials and Interfaces,* 8, 4532-4540.

[27] Garain, S., Sinha, T. K., Adhikary, P., & Henkel, K. (2015). Self-Poled Transparent and Flexible UV Light-Emitting Cerium Complex-PVDF Composite. *Applied Material and Interfaces*, 7, 1298-1307.

[28] Gautschi, G. (2002). Piezoelectric Sensors. *In: Piezoelectric Sensorics. Springer, Berlin, Heidelberg*, 73-91.

[29] Ghosh, D., Giri, S., Sahoo, S., & Das, C. K. (2013). In situ synthesis of graphene/amine-modified graphene, polypyrrole composites in presence of srtio3 for supercapacitor applications. *Polymer-Plastics Technology and Engineering,* 52, 213-220.

[30] Hansen, B. J., Liu, Y., Yang, R., & Wang, Z. L. (2010). Hybrid nanogenerator for concurrently harvesting biomechanical and biochemical energy. *ACS Nano*, 4(7), 3647–3652.

[31] Harper, D. Piezoelectric. Online Etymology Dictionary.

[32] Hasegawa, D., Sheng, J. Y., Greenberg, D. A., & Thompson K. R. (2011). Far-field effects of tidal energy extraction in the Minas Passage on tidal circulation in the Bay of Fundy and Gulf of Maine using a nested-grid coastal circulation model. *Ocean Dynamics,* 61, 1845-1868.

[33] Henkel, K., Lazareva, I., Mandal, D., Paloumpa, I., Müller, K., & Koval, Y. (2009). Electrical investigations on metal/ferroelectric/insulator/semiconductor structures using poly[vinylidene fluoride trifluoroethylene] as ferroelectric layer for organic nonvolatile memory applications. *Journal of Vacuum Science & Technology B*, 27, 504–507.

[34] Hillenbrand, J., Kodejska, M., Garcin, Y., Seggern, H., & Sessler G. M. (2010). High-sensitivity Piezoelectrect-film Accelerometers. *IEEE Transactions on Dielectrics and Electrical Insulation,* 17(4), 1021-1027.

[35] Holler, F. J., Skoog, D. A., & Crouch, S. R. (2007). Chapter 1. Principles of Instrumental Analysis (6th ed.). *Cengage Learning*, 9.

[36] Holmes-Siedle, A. Wilson, P., & Verrall, A. (1984). PVdF: An electronically-active polymer for industry. *Materials & Design*, 4(6), 910-918.

[37] Hong, B. (2008). Simple preparation of affinity membrane by using electrospinning and its protein adsorption characteristic. *Ph.D. Thesis of Keimyung University*, 12.

[38] Hoque, N., Thakur, P., Roy, S., Kool, A., & Bagachi, B. (2017). Er^{3+}/Fe^{3+} Stimulated Electroactive, Visible Light Emitting, and High Dielectric Flexible PVDF Film Based Piezoelectric Nanogenerators. *Applied Materials and Interfaces*, 9, 23048-23059.

[39] Juan, P., Yan, X. J., Jiang, Y. D., Chang, C., & Lin, L. W. (2010). Piezoelectric actuation of direct-write electrospun fibers. *Sensors and Actuators A: Physical*, 164, 131-136.

[40] Krautkrämer, J. & Krautkrämer, H. (1990). Ultrasonic Testing of Materials. *Springer*, 4, 117-140.

[41] Kumar, P. (2013). Piezo-Smart Rods. *International Journal of Enhanced Research in Science Technology & Engineering,* 2(6), 65-70.

[42] Lakes, R. Electrical Properties of Bone: A Review. University of Wisconsin–Madison.

[43] Lanceros-Mendez, S., Mano, J., Costa, A., & Schmidt, V. (2001). FTIR and DSC studies of mechanically deformed β-PVDF films. *Journal of Macromolecular Science, Part B*, 40, 517-527.

[44] Li, D., & Xia, Y. (2004). Electrospinning of Nanofibers: Reinventing the Wheel? *Advanced Materials*, 16, 1151-1170.

[45] Lin, Z. H., Yang, Y., Wu, J. M., Liu, Y., Zhang, F., & Wang, Z. L. (2012). BaTiO3 Nanotubes-Based Flexible and Transparent Nanogenerators. *The Journal of Physical Chemistry Letters*, 3(23), 3599-3604.

[46] Liu, Z., Pan, C. T., Lin, L. W., & Lai, H. W. (2013). Piezoelectric properties of PVDF/MWCNT nano-fiber using near-field electrospinning. *Sensors and Actuators A: Physical*, 193,13–24.

[47] Lovinger, A. J. (1983). Ferroelectric Polymers. *Science Magazine*, 220(4602),1115-1121.

[48] Manbachi, A. & Cobbold, R.S.C. (2011). Development and Application of Piezoelectric Materials for Ultrasound Generation and Detection. *Ultrasound, SAGE Journals,* 19 (4), 187–196.

[49] Mandal, D., Henkel, K., & Schmeißer, D. (2012). The electroactive β-phase formation in Poly(vinylidene fluoride) by gold nanoparticles doping. *Materials Letters,* 73, 123–125.

[50] Mao, Y., Zhao, P., McConohy, G., Yang, H., Tong, Y., & Wang, X. (2014). Sponge-Like Piezoelectric Polymer Films for Scalable and Integratable Nanogenerators and Self-Powered Electronic Systems. *Advanced Energy Materials*, 4, 1301624−1301631.

[51] McKinney, J. E., Davis, G. T., & Broadhurst, M. G. (1980). Plasma poling of poly(vinylidene fluoride): Piezo- and pyroelectric response. *Journal of Applied Physics,* 51, 1676.

[52] Minary-Jolandan, M. & Yu, M. (2009). Nanoscale characterization of isolated individual type I collagen fibrils: Polarization and piezoelectricity. *Nanotechnology*. 20(8), 085706.

[53] Mishra, S., Lakshmi, U., Kumar, S. K., & Mohanty, S. (2018). Advances in Piezoelectric Polymer Composites for Energy Harvesting Applications: A Systemic Review. *Macromolecular Materials and Engineering, 180046,* 1-25.

[54] Nakamura, K., Sawai, D., & Watanabe, Y. (2003). Effect of annealing on the structure and properties of poly (vinylidene fluoride) β-form films. *Journal of Polymer Science Part B*, 41, 1701-1712.

[55] Narita, F., & Fox, M. (2018). A Review on Piezoelectric, Magnetostrictive, and Magnetoelectric Materials and Device Technologies for Energy Harvesting Applications. *Advance Engineering Materials Journal*, 20, 1700743.

[56] Nilsson, E., Lund, A., Jonasson, C., Jonasson, C., Hagstrom, B. (2013). Poling and characterization of piezoelectric polymer fibers for use in textile sensors. *Sensors and Actuators A: Physical,* 201, 477-486.

[57] Padron, S., Fuentes, A., Caruntu, D., & Lozano, K. (2013). Experimental Study of Nanofiber Production Through Forcespinning. *Journal of Applied Physics,* 113, 024318.

[58] Pi, Z., Zhang, J., Wen, C., Zhang, Z., & Wu, D. (2014). Flexible piezoelectric nanogenerator made of poly(vinylidenefluoride-co-trifluroethylene) (PVDF-TrFE) thin film. *Nano Energy,* 7, 33-41.

[59] Qu, Q., Yang, S., & Feng, X. (2011). 2-D sandwich-like sheets of iron oxide grown on graphene as high energy anode material for supercapacitors. *Advanced Materials,* 23, 5574-5580.

[60] Radusinović, D., & Markov, C. (1971). Macedonite – lead titanate: a new mineral (PDF). *American Mineralogist*, 56, 387-394.

[61] Ramakrishna, S., Fujihara, K., Teo, W., Lim, T., & Ma, Z. (2005). An Introduction to Electrospinning and Nanofiber. *NJ World Scientific Publishing Co., Hackensack, Singapore*.

[62] Safari, A. & Akdogan, E. (2008). *Piezoelectric and Acoustic Materials for Transducer Applications, Springer*, 387–394.

[63] Salimi, A., & Yousefi, A. (2003). Analysis Method: FTIR studies of β-phase crystal formation in stretched PVDF films. *Polymer Testing,* 22(6), 699-704.

[64] Salimi, A., & Yousefi, A. (2004). Conformational changes and phase transformation mechanisms in PVDF solution-cast films. *Journal of Polymer Science Part B,* 42(18), 3487-3495.

[65] Scanning Electron Microscopy. NanoScience Instruments (2019). Image obtained from https://www.nanoscience.com/techniques/scanning-electron-microscopy/

[66] Sharma, T., Je, S., Gill, B., & Zhang, J. X. J. (2011). Patterning piezoelectric thin film PVDF-TrFE based pressure sensor for catheter application. *Sensors and Actuators A: Physical,* 177, 87-92.

[67] Snook, G. A., Kao, P., Best, A. S. (2011). Conducting-polymer-based supercapacitor devices and electrodes. *Journal of Power Sources,* 196, 1-12.

[68] Soin, N., Shah, T. H., Anand, S. C., Geng, J., Pornwannachai, W., Mandal, P., Reid, D., Sharma, S., Hadimani, R. L., Bayramol, D. V., & Siores, E. (2014). Novel "3-D Spacer" All Fibre Piezoelectric Textiles for Energy Harvesting Applications. *Energy & Environmental Science*, 7, 1670−1679.

[69] Thakur, V. K., Tan, E. J., Lin, M. F., & Lee, P. S. (2011). Polystyrene grafted polyvinylidene fluoride copolymers with high capacity performance. *Polymer Chemistry,* 2, 2000-2009.

[70] Ting, Y., Gunawan, H., Sugondo, A., & Chiu, C. (2013). A New Approach for Polyvinylidene Fluoride (PVDF) Poling Method for Higher Electric Response. *Ferroelectrics,* 446, 28-38.

[71] Trolier-McKinstry, S. (2008). Crystal Chemistry of Piezoelectric Materials. *In: Safari A., Akdoğan E.K. (eds) Piezoelectric and Acoustic Materials for Transducer Applications. Springer, Boston, MA,* 39-56.

[72] Ueberschlag, P. (2001). PVDF piezoelectric polymer. *Sensor Review,* 21(2), 118-125.

[73] Vazquez, B., Vasquez, H., & Lozano, K. (2012). Preparation and Characterization of Polyvinylidene Fluoride Nanofibrous Membranes by Forcespinning™. *Polymer Engineering and Science*, 52(10), 2260-2265.

[74] Wang, X., Yang, B., Liu, J., Zhu, Y., Yang, C., & He, Q. (2016). A flexible triboelectric-piezoelectric hybrid nanogenerator based on P(VDF-TrFE) nanofibers and PDMS/MWCNT for wearable devices. *Scientific Reports,* 6(36409), 1-10.

[75] Wang, Z. L., & Song, J. (2006). Piezoelectric Nanogenerators Based on Zinc Oxide Nanowire Arrays. *Science*, 312, 242−246.

[76] Wang, Z. L., Zhu, G., Yang, Y., Wang, S., & Pan, C. (2012). Progress in Nanogenerators for Portable Electronics. *Materials Today*, 15(12), 532−543.

[77] Xin, Y., Qi, X., Tian, H., Gou, C., Li, X., Lin, J., & Wang., C. (2015). Full-fiber piezoelectric sensor by straight PVDF/nanoclay nanofibers. *Materials Letters,* 164, 136-139.

[78] Yang, J. H., Ryu, T., Lansac, Y., Jang, Y. H., & Lee, B. H. (2016). Shear stress-induced enhancement of the piezoelectric properties of PVDF-TrFE thin films. *Organic Electronics*, 28, 67-72.

[79] Yee, W., Kotaki, M., Liu, Y., & Lu, X. (2007). Morphology, polymorphism behavior and molecular orientation of electrospun poly (vinylidene fluoride) nanofibers. *Polymer*, 48(2), 512-521.

BIOGRAPHICAL SKETCH

My name is Misael Eduardo Martinez, and I am a Mechanical Engineering Master Student at the University of Texas Rio Grande Valley in Edinburg, TX. I was born in McAllen, TX, in February of 1995; although I was born in the United States, I lived most of my life in Reynosa, Tamaulipas, Mexico. I started my studies in Mexico where I finished elementary and middle school. In 2010, I moved to Pharr, TX, where I went to Valley View High School. While pursuing my high school degree, I obtained my degree in Interdisciplinary Studies from South Texas College along with my High School graduation diploma in 2014.

In August 2014, I entered to the University of Texas Pan American in Edinburg, TX, to pursue my Bachelor's in Mechanical Engineering. During this time, I participated in numerous student organizations such as SHPE, ASME, Material Advantage, SWE, TexPREP, etc. I also had the opportunity to participate in an Undergraduate Research Experience with the University Transportation Center for Railway Safety in College Station, TX for the summer of 2016. I also got the opportunity to start researching nanomaterials for different applications starting January 2017, till the present. In May 2017, I graduated from the University of Texas Rio Grande Valley (formerly UTPA) with my bachelor's degree in Mechanical Engineering. That summer I entered the Mechanical Engineering Master program, specializing in Material Science. After two years of researching on different nanomaterials for a wide variety of applications, I will graduate on May 2019 with my master's degree. If you wish contact me, you may do so at my personal email, misaelmtz95@gmail.com.